CHARACTERIZATION AND MODELING OF THORACO-ABDOMINAL RESPONSE TO BLAST WAVES

Volume 6. Biomechanical Model of Lung Injury Mechanisms

Annual/Final Report

May 1985

C. J. Chuong

JAYCOR
11011 Torreyana Road
San Diego, California 92121

Contract No. DAMD17-82-C-2062

Supported by

U. S. Army Medical Research and Development Command
Fort Detrick, Frederick, Maryland 21701

The findings in this report are not to be construed as an official Department of the Army position unless so designated by other authorized documents.

SECURITY CLASSIFICATION OF THIS PAGE

ADA190811

REPORT DOCUMENTATION PAGE

Form Approved OMB No. 0704-0188

1a. REPORT SECURITY CLASSIFICATION UNCLASSIFIED	1b. RESTRICTIVE MARKINGS
2a. SECURITY CLASSIFICATION AUTHORITY	3. DISTRIBUTION/AVAILABILITY OF REPORT Approved for public release; distribution unlimited
2b. DECLASSIFICATION/DOWNGRADING SCHEDULE	
4. PERFORMING ORGANIZATION REPORT NUMBER(S)	5. MONITORING ORGANIZATION REPORT NUMBER(S)
6a. NAME OF PERFORMING ORGANIZATION JAYCOR 6b. OFFICE SYMBOL (If applicable)	7a. NAME OF MONITORING ORGANIZATION
6c. ADDRESS (City, State, and ZIP Code) 11011 Torreyana Road San Diego, California 92121	7b. ADDRESS (City, State, and ZIP Code)
8a. NAME OF FUNDING/SPONSORING ORGANIZATION U.S. Army Medical Research & Development Command 8b. OFFICE SYMBOL (If applicable)	9. PROCUREMENT INSTRUMENT IDENTIFICATION NUMBER DAMD17-82-C-2062
8c. ADDRESS (City, State, and ZIP Code) Fort Detrick Frederick, Maryland 21701-5012	10. SOURCE OF FUNDING NUMBERS PROGRAM ELEMENT NO. 61102A; PROJECT NO. 3M1 61102BS10; TASK NO. CG; WORK UNIT ACCESSION NO. 087

11. TITLE (Include Security Classification)
(U) Characterization and Modeling of Thoraco-Abdominal Response to Blast Waves
Volume 6. Biomechanical Model of Lung Injury Mechanisms

12. PERSONAL AUTHOR(S)
C. J. Chuong

13a. TYPE OF REPORT	13b. TIME COVERED	14. DATE OF REPORT (Year, Month, Day)	15. PAGE COUNT
Annual/Final	FROM 2/15/82 TO 5/31/85	1985 May	52

16. SUPPLEMENTARY NOTATION
Annual covers time period of 15 February 1984 - 31 May 1985.
Annual/Final published in 8 volumes

17. COSATI CODES			18. SUBJECT TERMS (Continue on reverse if necessary and identify by block number)
FIELD	GROUP	SUB-GROUP	
06	21		
06	17		

19. ABSTRACT (Continue on reverse if necessary and identify by block number)

20. DISTRIBUTION/AVAILABILITY OF ABSTRACT ☐ UNCLASSIFIED/UNLIMITED ☒ SAME AS RPT. ☐ DTIC USERS	21. ABSTRACT SECURITY CLASSIFICATION Unclassified
22a. NAME OF RESPONSIBLE INDIVIDUAL Mary Frances Bostian	22b TELEPHONE (Include Area Code) 301-663-7325
	22c. OFFICE SYMBOL SGRD-RMI-S

DD Form 1473, JUN 86 Previous editions are obsolete. SECURITY CLASSIFICATION OF THIS PAGE

FOREWORD

This Annual/Final Report has eight volumes. The titles are as follows:

1. Project Summary
2. Blast Load Definition on a Torso Model
3. Lung Dynamics and Mechanical Properties Determination
4. Biomechanical Model of Thorax Response to Blast Loading
5. Experimental Investigation of Lung Injury Mechanism
6. Biomechanical Model of Lung Injury Mechanisms
7. Gastrointestinal Response to Blast
8. Effect of Clothing on Thoracic Response

CONTENTS

ILLUSTRATIONS

TABLE

1. INTRODUCTION

A major objective of the Blast OverPressure (BOP) program is to understand blast injury. This includes the injury mechanisms, theories of tissue failure, determination of tissue failure strength, and prevention. With finite element model simulation, for a given blast wave loading, we are able to predict the intrathoracic overpressure histories at various points in the lung [13]. Questions arising are:

- What insightful information does the model prediction provide on the origin of injury?
- How do we correlate the actual blast injury with the local overpressure predictions?

This report documents our efforts toward these objectives. A review of lung trauma following blast wave exposure and impact is made in Section 2. It provides a summary of lung injury descriptions in both macroscopic and microscopic terms. With this background, we then look at the model simulation of wave dynamics in the lung, identify wave propagation characteristics. A comparison between lung hemorrhage and model overpressure prediction is made.

Typical patterns of lung blast injury are that (1) injury often starts to occur at the superficial layer of the pleura, (2) injuries are often seen as "rib-marking." Section 3 presents a local model to look into the pleural surface wave dynamics. Larger inertial force of the bony rib can result in local indentation on the lung parenchyma at the pleural surface of the impact side. Due to wave reflection from the relatively solid wall of chest, lung parenchyma at the pleural surface can experience higher overpressure compared to an interior point. At the pleural surface, parenchyma next to a bony rib can experience even higher overpressure compared to that next to intercostal muscle because of more effective wave reflection.

2. A REVIEW OF LUNG TRAUMA FOLLOWING BLAST WAVE EXPOSURE AND IMPACT

A body is under mechanical stress when it is exposed to external mechanical loading. For a living biological body various physiological functions can also be disturbed or damaged if the induced mechanical stress is beyond the sustaining tolerance of the tissue. Since the Second World War there have been various studies, clinical and experimental, in an effort to understand different aspects of blast injuries; e.g., mechanism, lethality, diagnosis, treatment, prevention, and establishment of DRC under different blast environments. Systematic studies have been done by Zuckerman in Great Britain, Desaga in Germany, Clemedson and Jönsson in Sweden, and the group at the Lovelace Foundation of the United States, all aimed at the goal of understanding blast injuries.

In addition, the automobile industry expends effort in studying impact injury relating to the crashworthiness of vehicles. There are also several pathological case reports about human body free-fall into water following a suicide jump. Injuries or damage from these other trauma may be relevant to blast injuries. The purpose of this section is to summarize information gathered from a literature search on the lung trauma following blast waves or impact loading. The photos in this section are reproduced from the quoted references.

2.1 GROSS DESCRIPTION OF LUNG DAMAGE

Blast injuries without clear body surface wounds have been found to occur mostly in air-containing organs and usually showing blood-stained froth in the mouth, nose, and upper respiratory passages [11]. Common causes of death are associated with the formation of air or fibrous emboli that are believed to originate in the lung. Rupture of the visceral pleura, formation of pneumothorax, hemothorax, gross hemorrhage, and pulmonary edema are commonly used as gross descriptions of lung trauma.

Zuckerman's observation of lung damage after animal postmortem studies are summarized in Table 2-1.

Table 2-1. Gross Description of Zuckerman's Observations [11] on Lung Blast Injuries

Degree of Damage Severity	Gross Description	
	Surface View	Sectioned View
Very slight	Spot of hemorrhage on lung surface, often following the line of the ribs (Fig. 2-1).	Points of hemorrhage mostly occurred at a subpleural level.
Severe	Patches of hemorrhage of varying size (Fig. 2-2).	Localized and scattered hemorrhages occurred in relation to a large bronchial tube.
Very severe	The entire lung surface is hemorrhagic. Darker lines of hemorrhage were observed to follow the lines of the ribs and they were recognized against a background of lighter hemorrhage (Fig. 2-3).	Hemorrhage was seen to extend through the entire lung substance (Fig. 2-4).
Most severe	Rupture of visceral pleura, superficial laceration along the lines of the ribs. Occurrence of hemothorax and pneumothorax.	

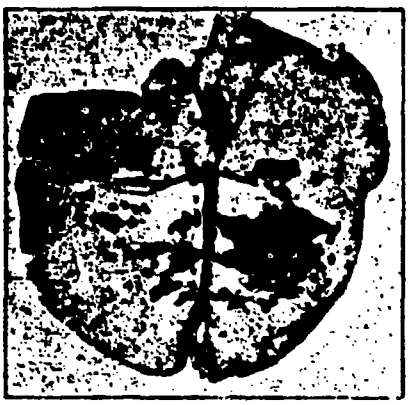

Figure 2-1. Lungs of a rabbit exposed to blast, showing small areas of hemorrhage, following the lines of the ribs [11].

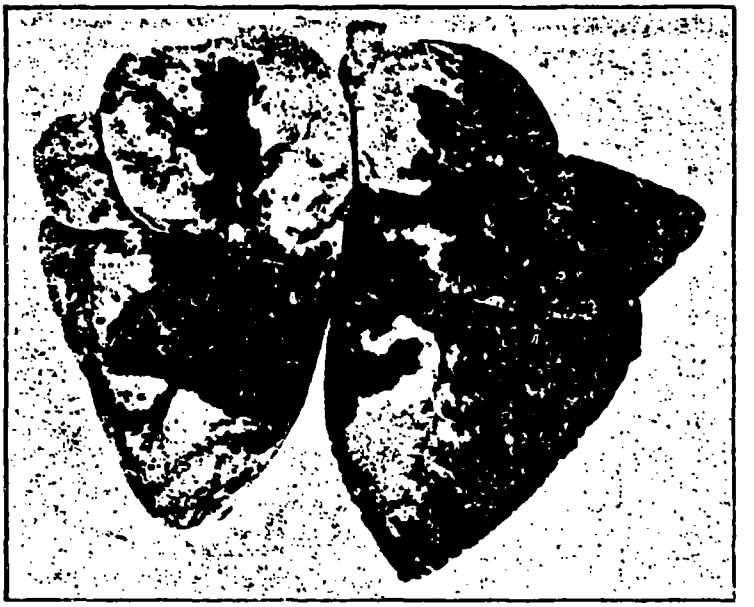

Figure 2-2. Lungs of a monkey exposed to blast, showing more extensive area of hemorrhage [11].

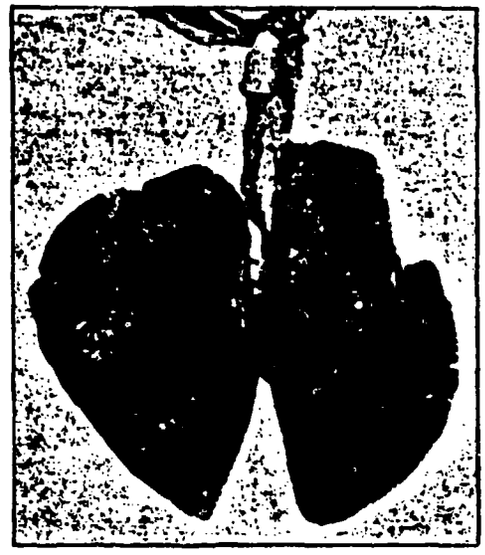

Figure 2-3. Very severe hemorrhages throughout the lungs of a rabbit exposed to blast [11].

Figure 2-4. Section through lung of a cat exposed to blast, showing extent of a zone of hemorrhage [11].

Zuckerman also noted the most vulnerable regions to be

1. The anterior and inferior borders,

2. The costal surface, especially the side closest to the explosion (Fig. 2-5),

3. The mediastinal surface of the lung.

Jönsson et al. [4] observed two types of impact injury depending on the magnitude and the rate of chest wall deformation from side impact experiments using rabbits. For velocities below 5 m/s with 50% chest wall deflection they observed lung tearing without significant hemorrhage. For velocities exceeding 10 m/s, however, severe hemorrhage was seen even when the chest wall deflection was less than 15%. The second type of injury is considered to be similar to that due to blast exposure. Lau et al. [5] confirmed the observation with rabbit sternal impact experiments. They described the first type damage as contusion of the bronchial region and the second type injury as contusion at both bronchial and aveolar regions.

Apparently, the first type injury, which is similar to the damage from quasi-static loading, is due to the great body deformation associated with large inward chest wall displacement. The second type injury, which is similar to the damage from high-strain-rate loading, is due to the propagation of stress waves characterized by the transient chest wall velocity. This has led to the suggestion that the chest wall velocity is a critical parameter in lung injury of this type.

2.2 MICROSCOPIC DESCRIPTION OF LUNG DAMAGE

The microscopic changes observed at the alveolar level when hemorrhage and edema occur are summarized below.

Zuckerman described that:

1. Capillary dilation occurred with exudation of fluid into many alveoli,

2. In severe cases with disrupted alveolar wall and torn capillaries, red cells appeared in the alveoli, small bronchioles, and interstitial hemorrhage occurred (Figs. 2-6 and 2-7),

3. In very severe cases, larger bronchioles were filled with blood.

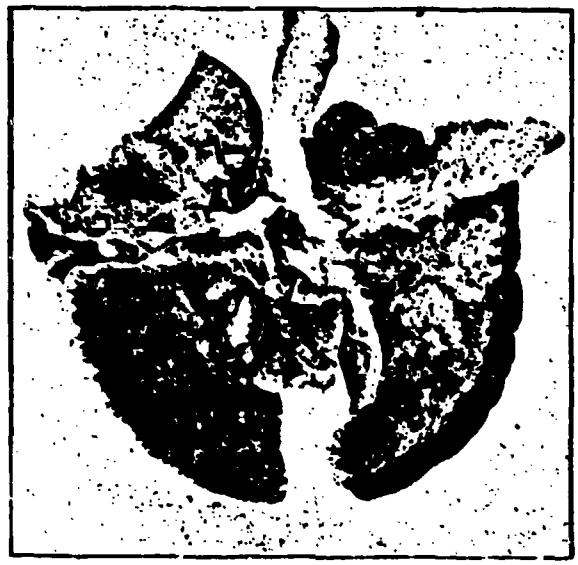

Figure 2-5. Lungs of a rabbit exposed close to the explosion of oxygen and hydrogen in a balloon. The hemorrhages are confined to the side closest to the explosion [11].

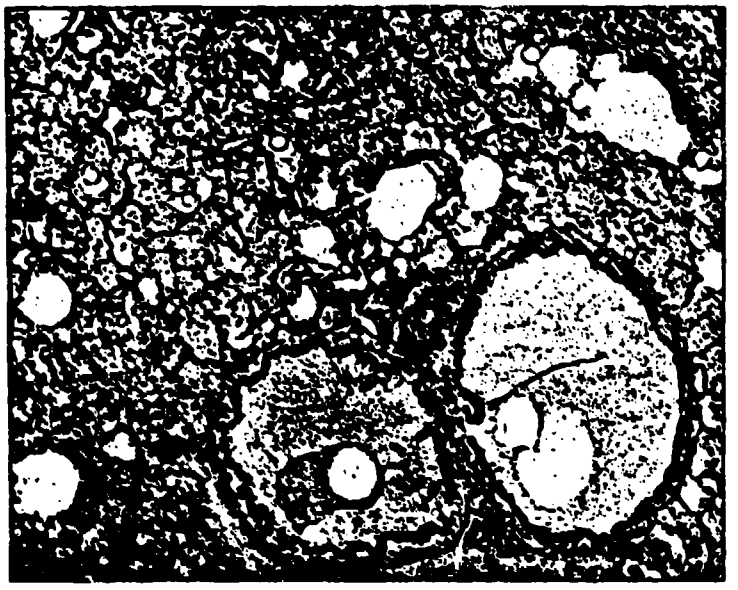

Figure 2-6. Section of a rabbit lung after exposure to blast. The alveoli and bronchioles are filled with blood (× 71) [11].

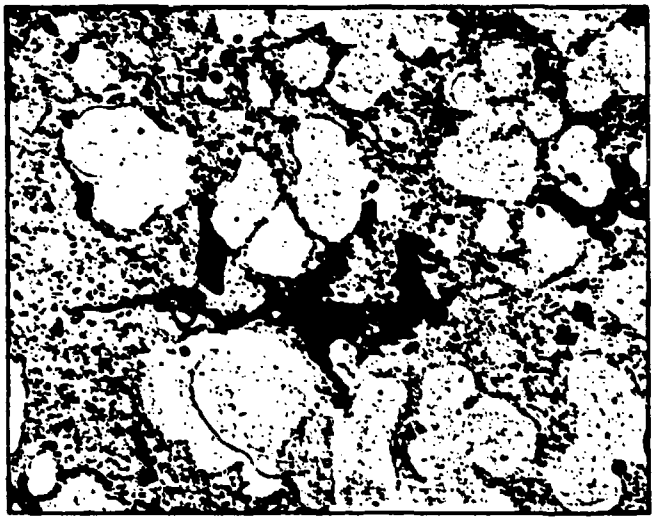

Figure 2-7. Section of the lungs of a woman killed in an air raid. The casualty was extricated from the remains of her house, and autopsy revealed numerour hemorrhages in both lungs. The specimen has been stained with scharlach R. (black regions) to demonstrate fat (× 58) (H.L.5) [11].

Webster et al. [10] performed pathology studies on traumatized lungs, including blast injured lungs. He described one or all of the following changes to lung parenchyma after trauma:

1. The lower respiratory tract is filled with edematous fluid.

2. Hemorrhage, in which the alveolar spaces are filled with red cells.

3. Desquamative alveolitis, in which the alveolar epithelial cells become swollen following basement membrane edema in the alveolar wall. The swollen alveolar epithelial cells are then shed into alveolar spaces (Fig. 2-8).

With electron microscopy he demonstrated the granularity of the endothelial cell with widening canals between the endothelial cells (Fig. 2-9). The plasma may then pass into the basement membrane and eventually into the alveolar spaces (Fig. 2-10). Following the edema of basement membrane, degenerative changes develop at epithelial cells resulting in swelling of these cells and subsequent desquamation which may be such as to fill the alveolar spaces.

Therefore, the integrity of the pulmonary structure and function, e.g., gas exchanges, biochemical equilibrium, surfactant secretion and elasticity of the alveolar wall, are damaged or disturbed. The last two changes can probably explain, at least in part, the reduction of lung compliance of rabbit lungs following air blast exposures [1].

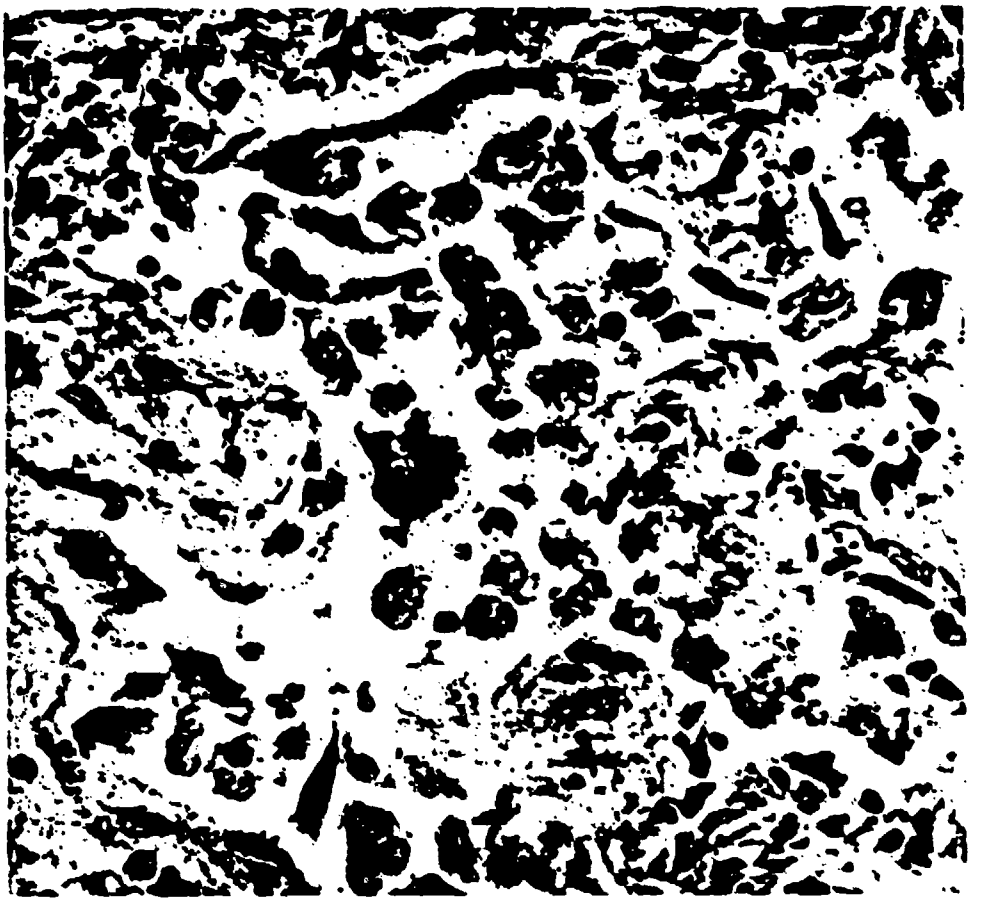

Figure 2-8. Section of lung one week after trauma showing the desquamation of the alveolar epithelial cells (200×) [10].

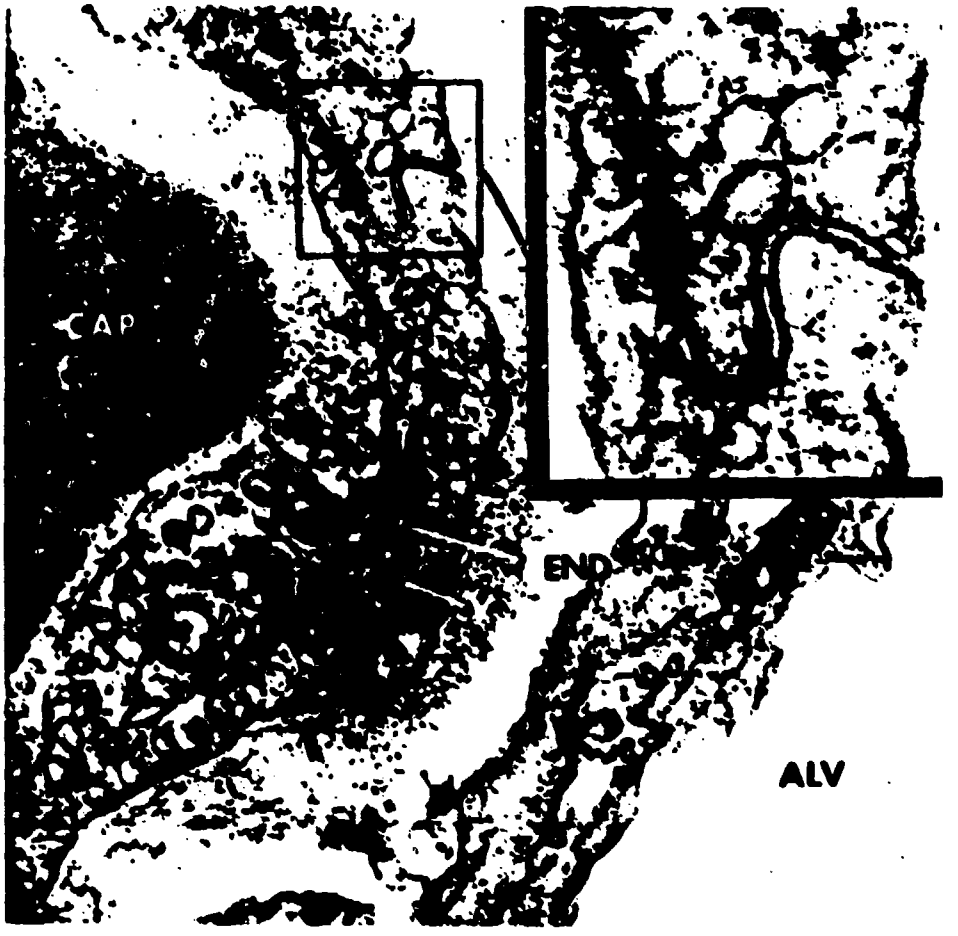

Figure 2-9. Ultrastructure of the capillary endothelium showing the gas transfer vesicles and intercellular canal (54,000×; inset 14,000×).

Legend: CAP, capillary; END, endothelial cell; V, vesicles; ALV, alveolar space [10].

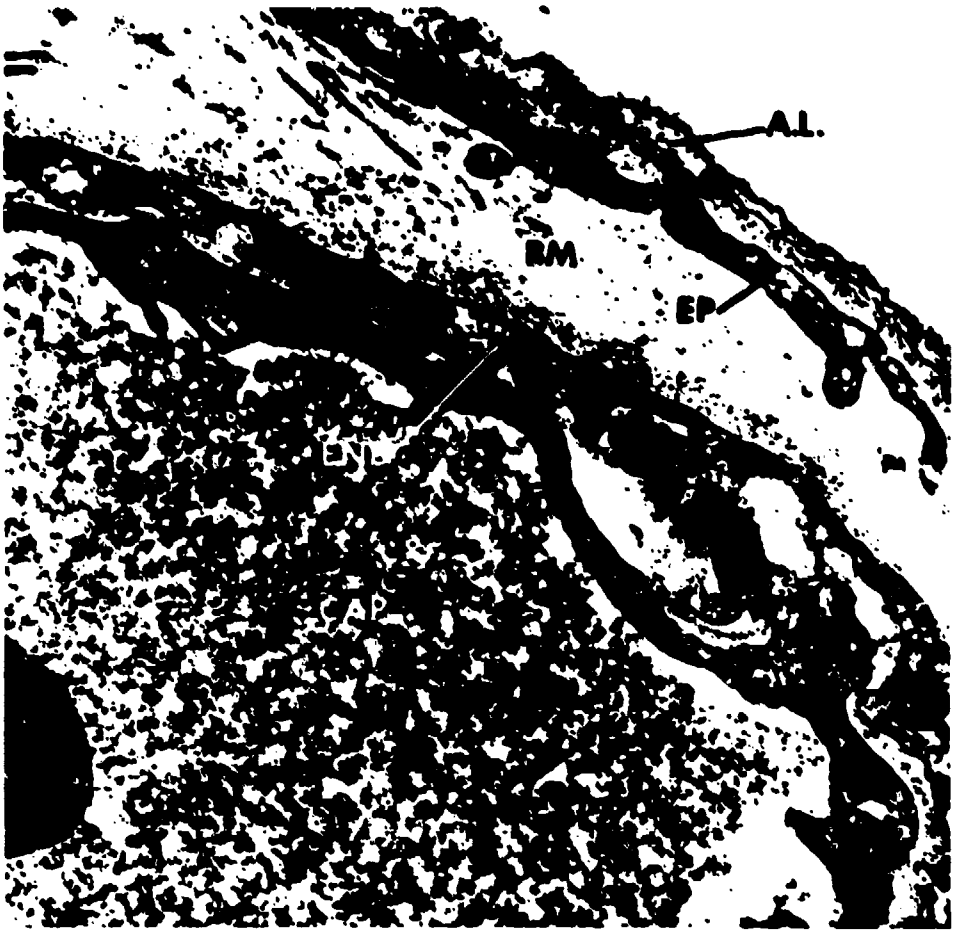

Figure 2-10. Ultrastructure of the alveolar wall (54,000×).

Legend: CAP, capillary; END, endothelial cell; BM, basement membrane; EP, alveolar epithelium; AL, alveolar lining. The basement membrane is edematous and the endothelial and epithelial cells are more granular than usual. The osmophilic and non-osmophilic layers of the alveolar lining are shown [10].

3. FINITE ELEMENT ANALYSIS OF WAVE DYNAMICS OF THE LUNG

Various clinical and experimental blast injury studies clearly demonstrate that lung hemorrhage tends to first appear at certain locations with certain characteristic patterns. The superficial layer of the pleural surface, especially the impact side, and that bordering the heart are identified as the regions most likely to have gross hemorrhage. The "rib marking" type hemorrhage is a characteristic pattern. The injury observation indicates that different parts of the lung experience different local loadings during the blast incidence, and wave dynamics may play an important role in the formation of damages.

A two-dimensional finite element model has been constructed to simulate the blast exposure of a sheep [13]. This model demonstrates the wave propagation characteristics inside the thorax during blast exposure. It predicts that tissues at different parts of the lung experience different wave loading histories to result in different local stress histories. The complex anatomical environments, geometric shapes, material properties, and body orientation to the direction of the incident wave can all complicate the wave dynamics to result in different loading histories inside the thorax.

The major contribution of a biomechanical model is, of course, to exhibit the underlying principles of mechanics which would otherwise be difficult to see from experiments. Limitations on experimental instruments and techniques can often restrict the availability of response data. Most of the past work was done under the assumption that uniform overpressure occurs in the lungs during blast exposure and it can be measured by esophageal pressure probes. Examination of injury patterns, certainly, does not support this concept. With the 2-D finite element model we can reasonably predict the esophageal pressure measurements under various loading conditions [13]. We can also exhibit the wave propagation characteristics as well as the different local overpressure distribution inside the thorax.

Understanding of tissue failure mechanisms under blast wave requires correlations between model prediction of tissue response and the actual damage

observation. The rest of this report summarizes our efforts toward this goal. Various comparisons are made on a qualitative basis.

3.1 SIMULATION OF WAVE PROPAGATION IN THE LUNG

In the following, we shall see the wave propagation in the lung as the 2-D FEM model is exposed to a blast wave of 45 psi peak pressure and 1 ms duration. The analysis is carried out for 30 ms since the experimental esophageal pressure measurement diminishes after 20 ms. At a given time step, distribution of lung overpressure will be shown. Different degrees of local overpressure inside the chest cavity is represented by different colors. Evolution of color contour lines is, therefore, an indication of wave motion as time increases. The airblast comes from the right side of the sheep. The anterior and posterior sides of the model correspond to the low and upper edges of the page, respectively (see Fig. 3-1).

For clarity the overpressure is shown for the lung with the rest of the organs removed. Clinical studies and animal blast experiments indicate that, in addition to the chest wall pleural, the pleural region near the heart can be injured easily. In the current analysis it corresponds to the concave region of the subplots. Following the onset of blast arrival at the right body surface, the sequences of wave propagation is summarized in the following (Fig. 3-2):

1. At 1.00 ms, the incident wave starts penetrating into the right side of the lung.

2. At 1.25 ms, we can see further progression of the incident wave front entering from the right side. The left side of the lung is now also under the incident compression wave entering from the left side of the body surface.

3. At 1.75 and 2.00 ms, high compression starts to be seen at the right pleural surface. Because of wave reflection from the body surface, the actual blast pressure exerting on the right body surface is twice of the free field value. In other words, a larger compression is delivered to the right pleural surface. Lung tissues at the superficial region are exposed to the "less filtered" or larger pressure loading than those at the interior.

4. From 2.0 through 2.75 ms, high compression is seen at the lower corners as well as the lung near the heart. The wave is reflected from the relatively solid wall of the heart, resulting in higher

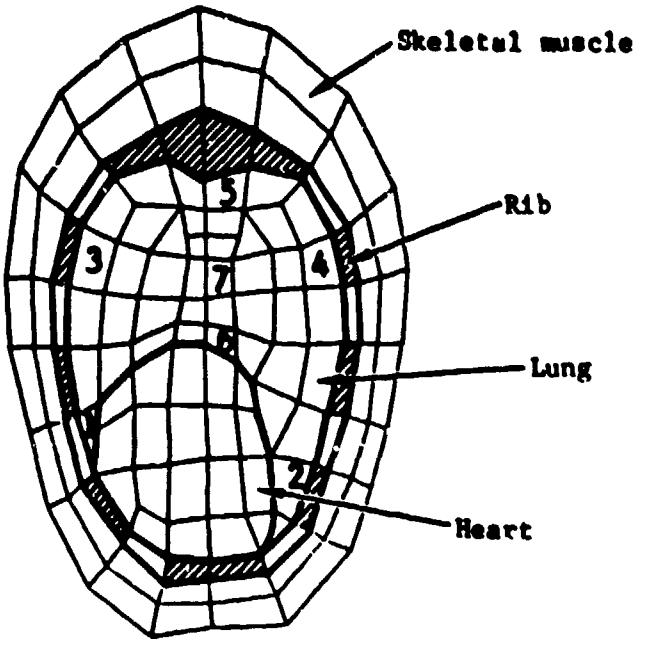

(a) FEM model

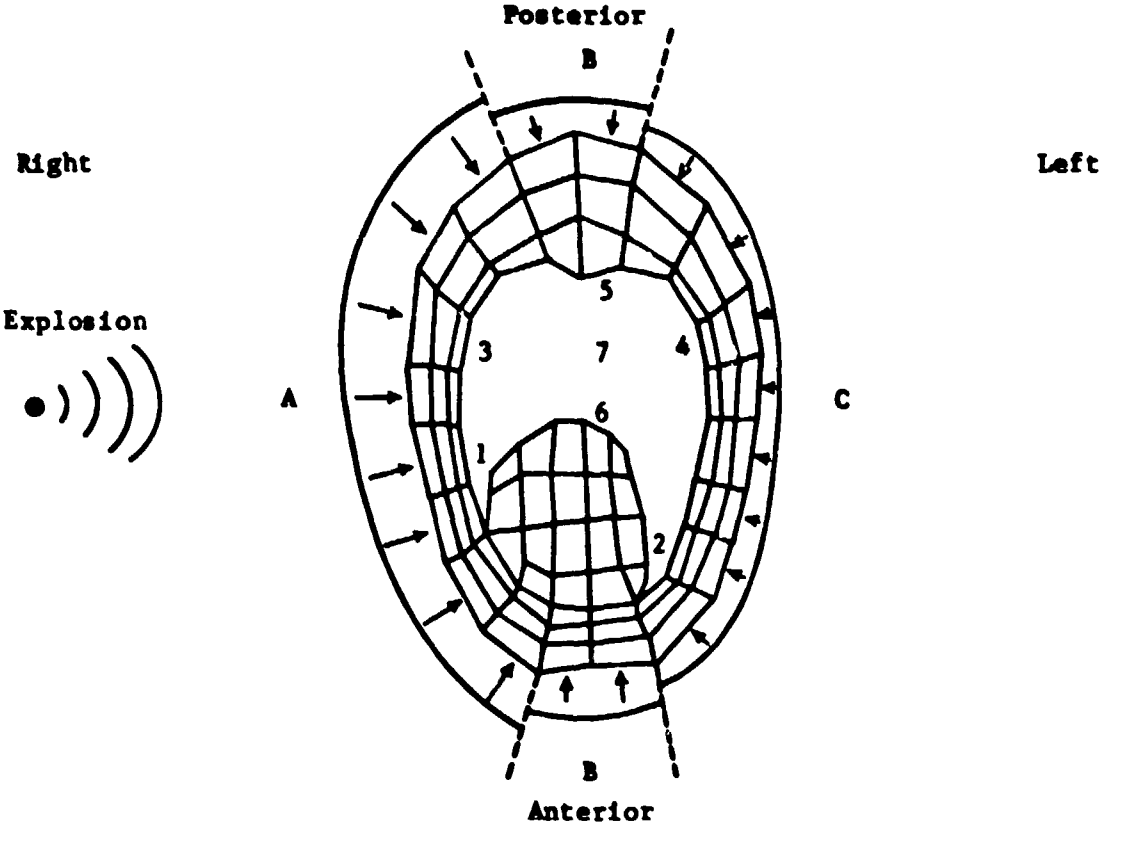

(b) Model body orientation to the explosion center

Figure 3-1. Finite element model and its body orientation to the explosion center. Zones A, B and C represent different degrees of blast loading increase due to wave reflection (see Ref. 13). Number labels in the lung region represent probe locations.

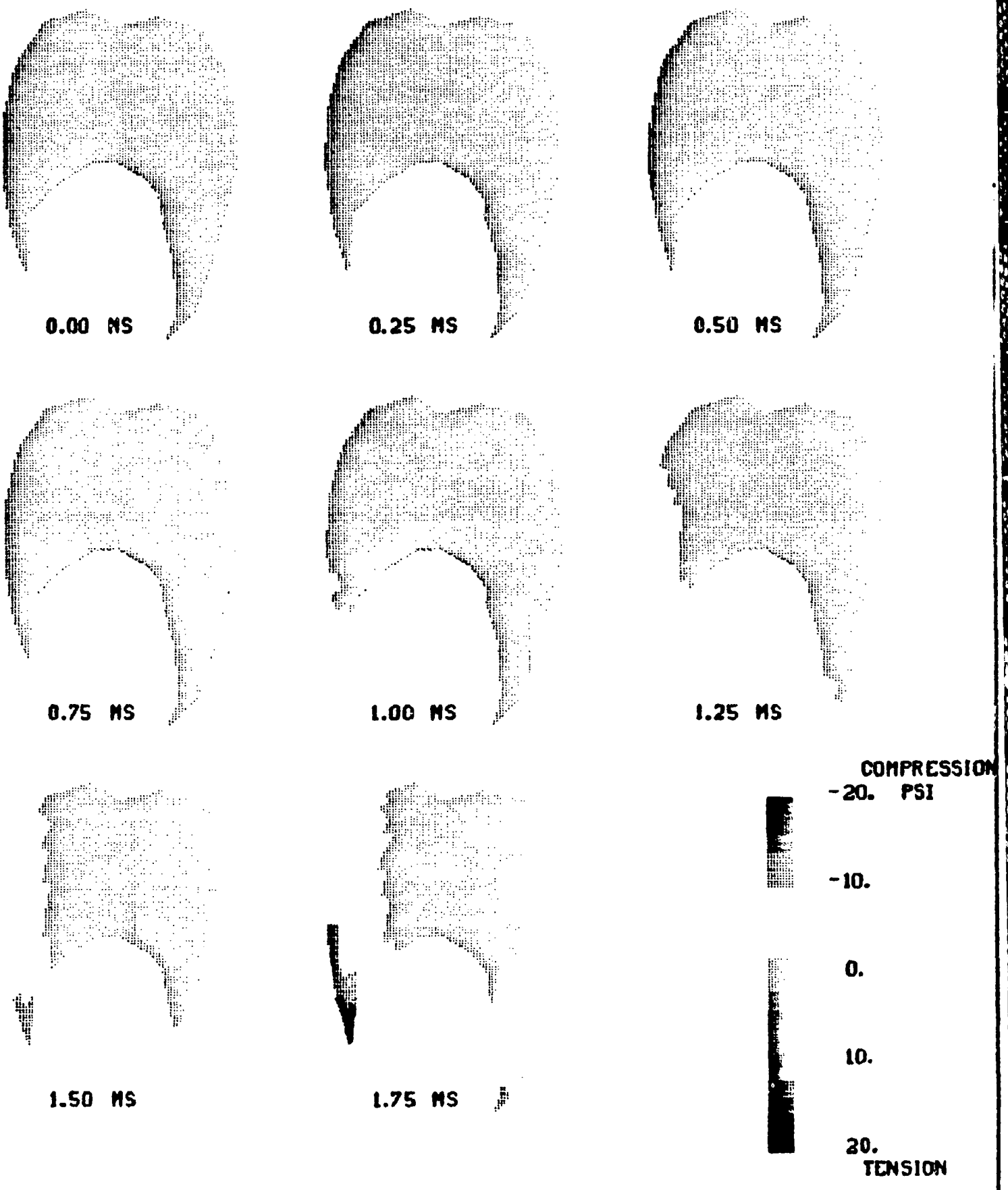

(a) Time 0.00-1.75 ms

Figure 3-2. Progression of compression waves in lung.

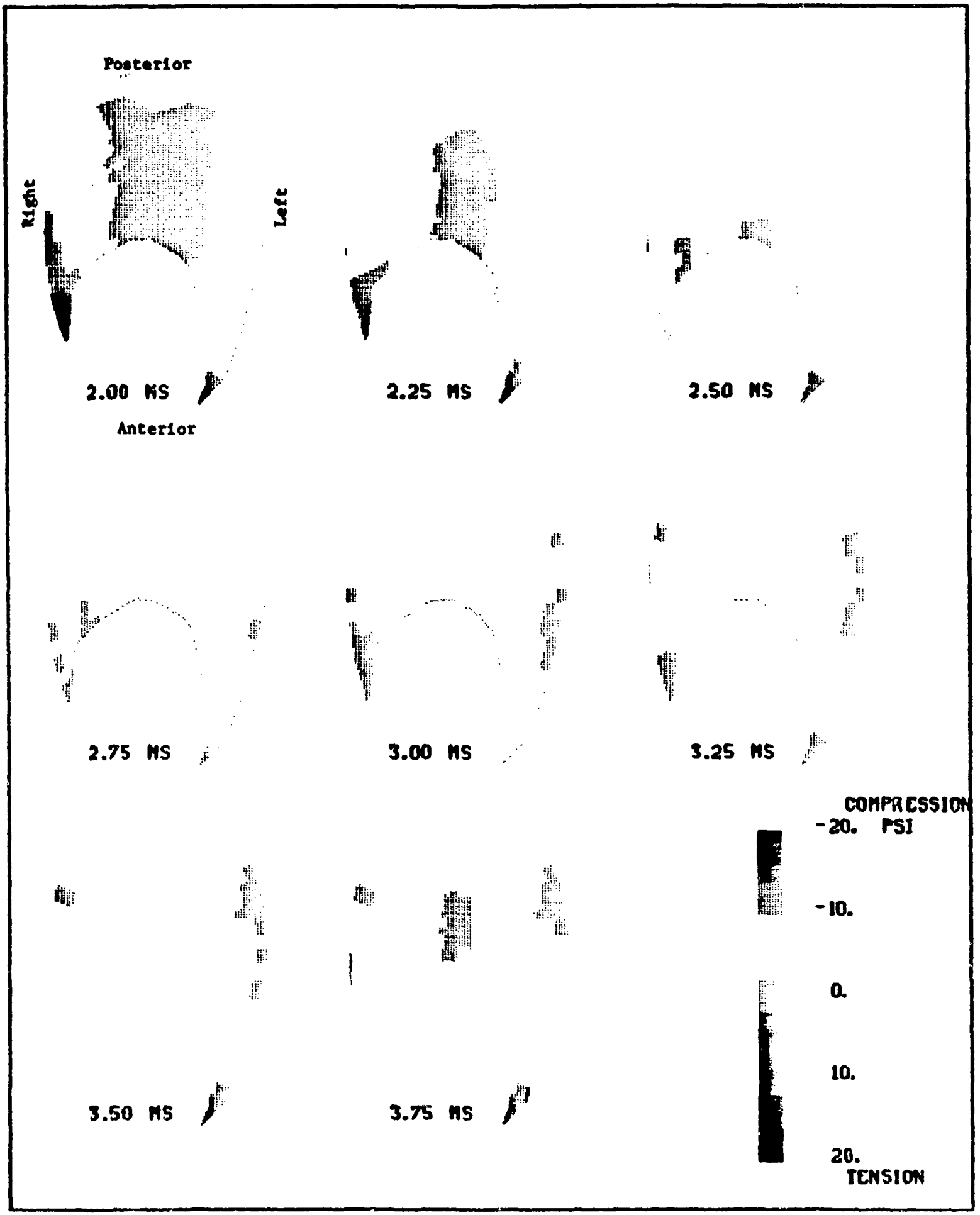

(b) Time 2.00-3.75 ms

Figure 3-2. (Cont'd)

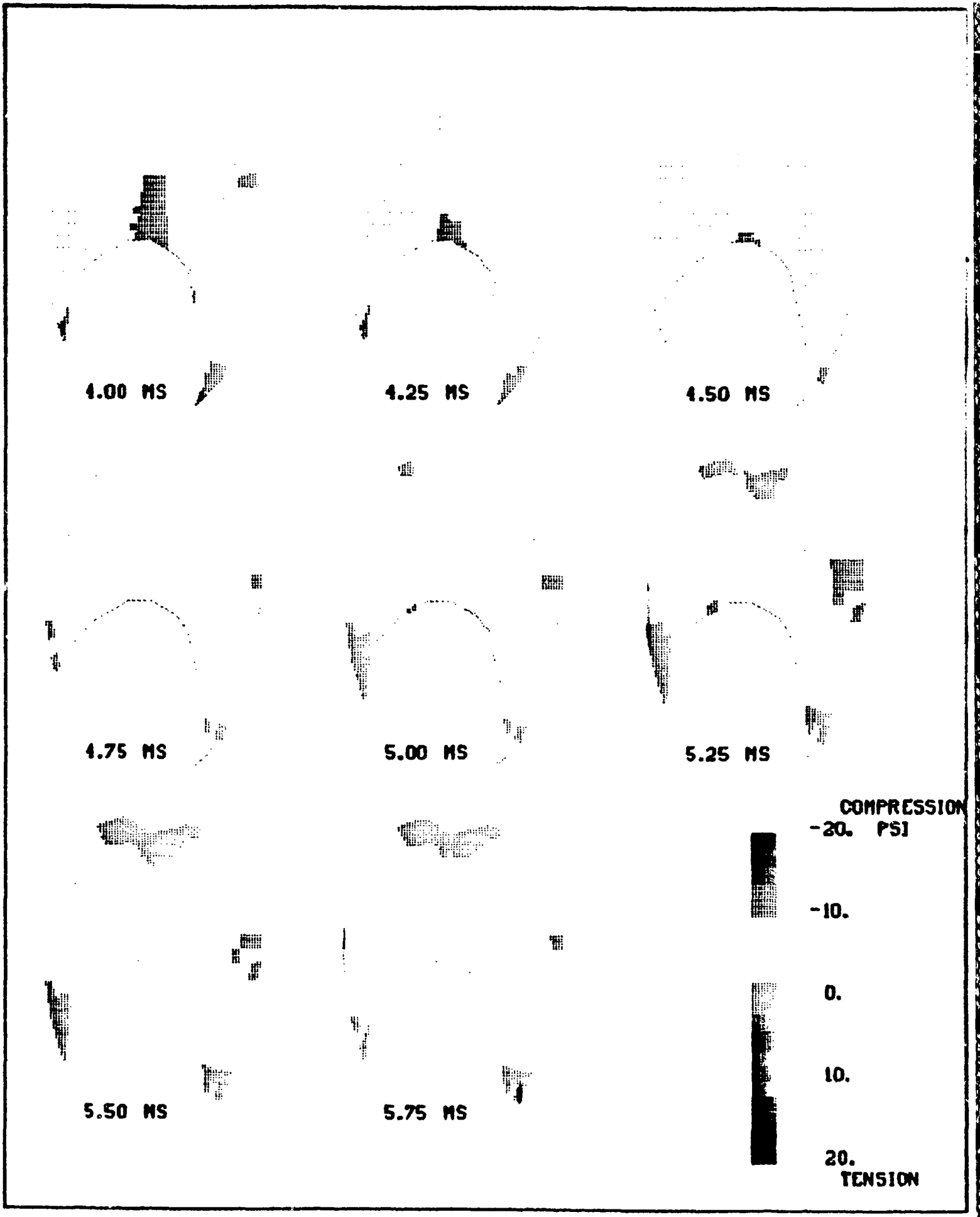

(c) Time 4.00-5.75 ms

Figure 3-2. (Cont'd)

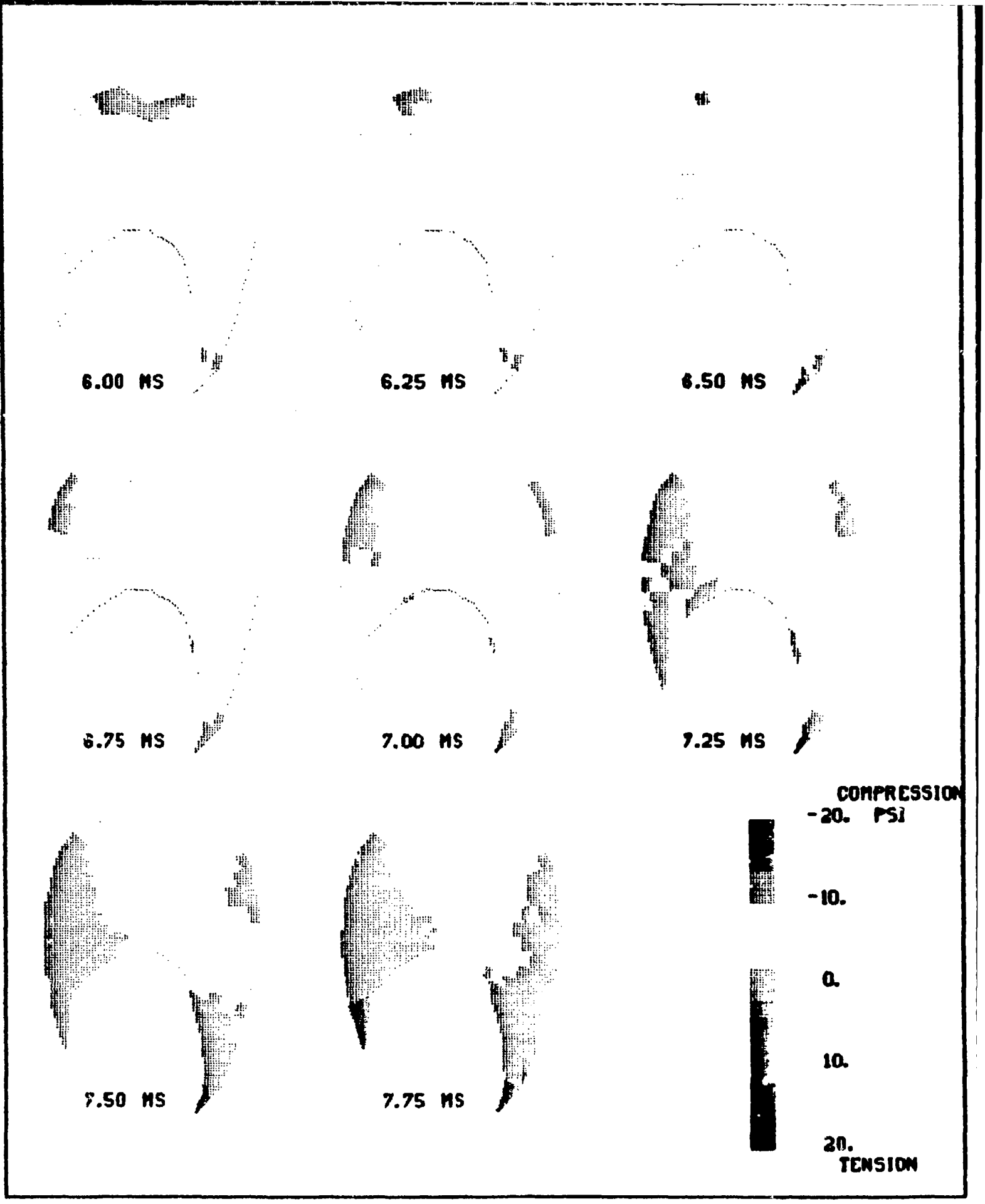

(d) Time 6.00-7.75 ms

Figure 3-2. (Cont'd)

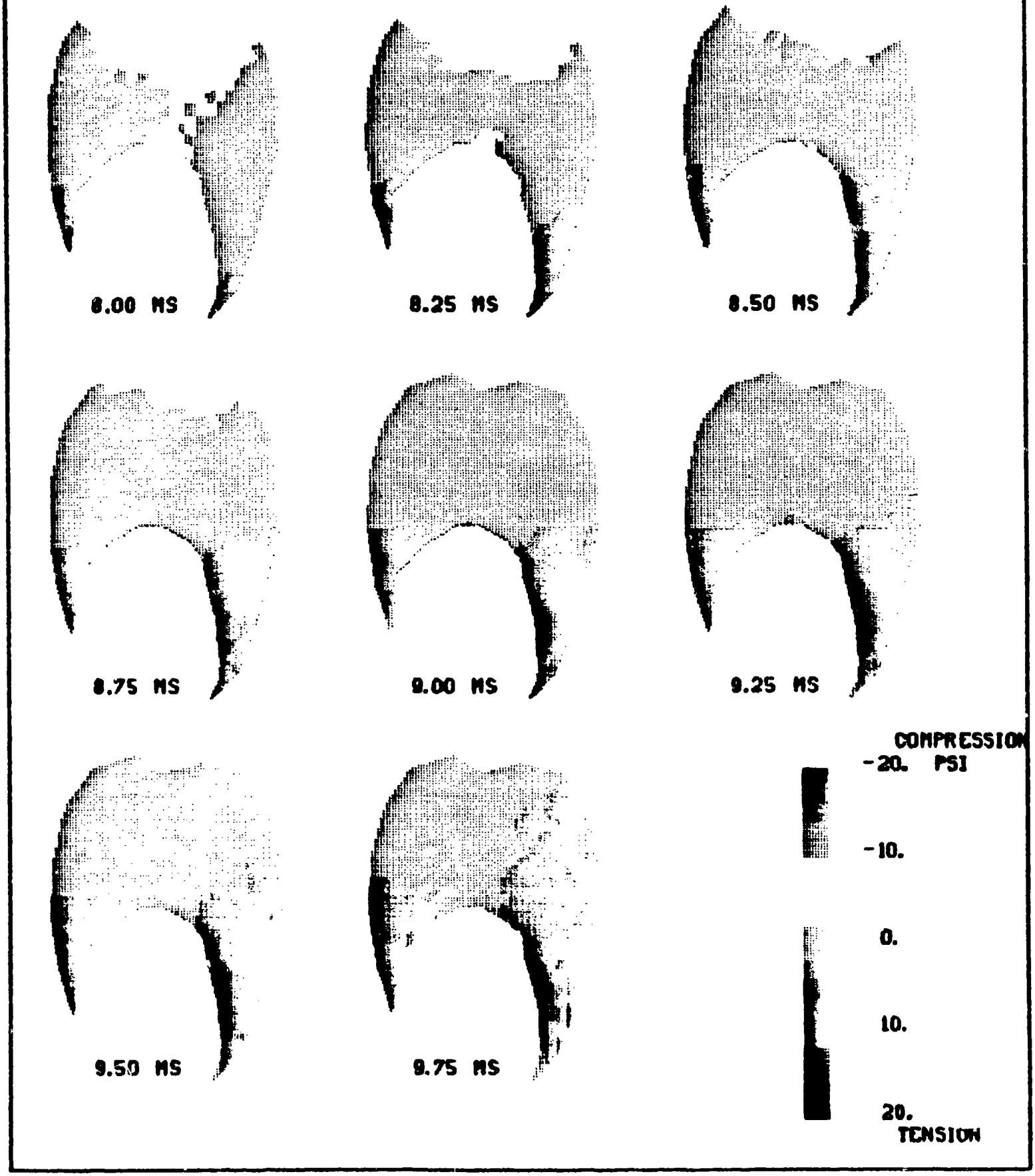

(e) Time 8.00-9.75 ms

Figure 3-2. (Cont'd)

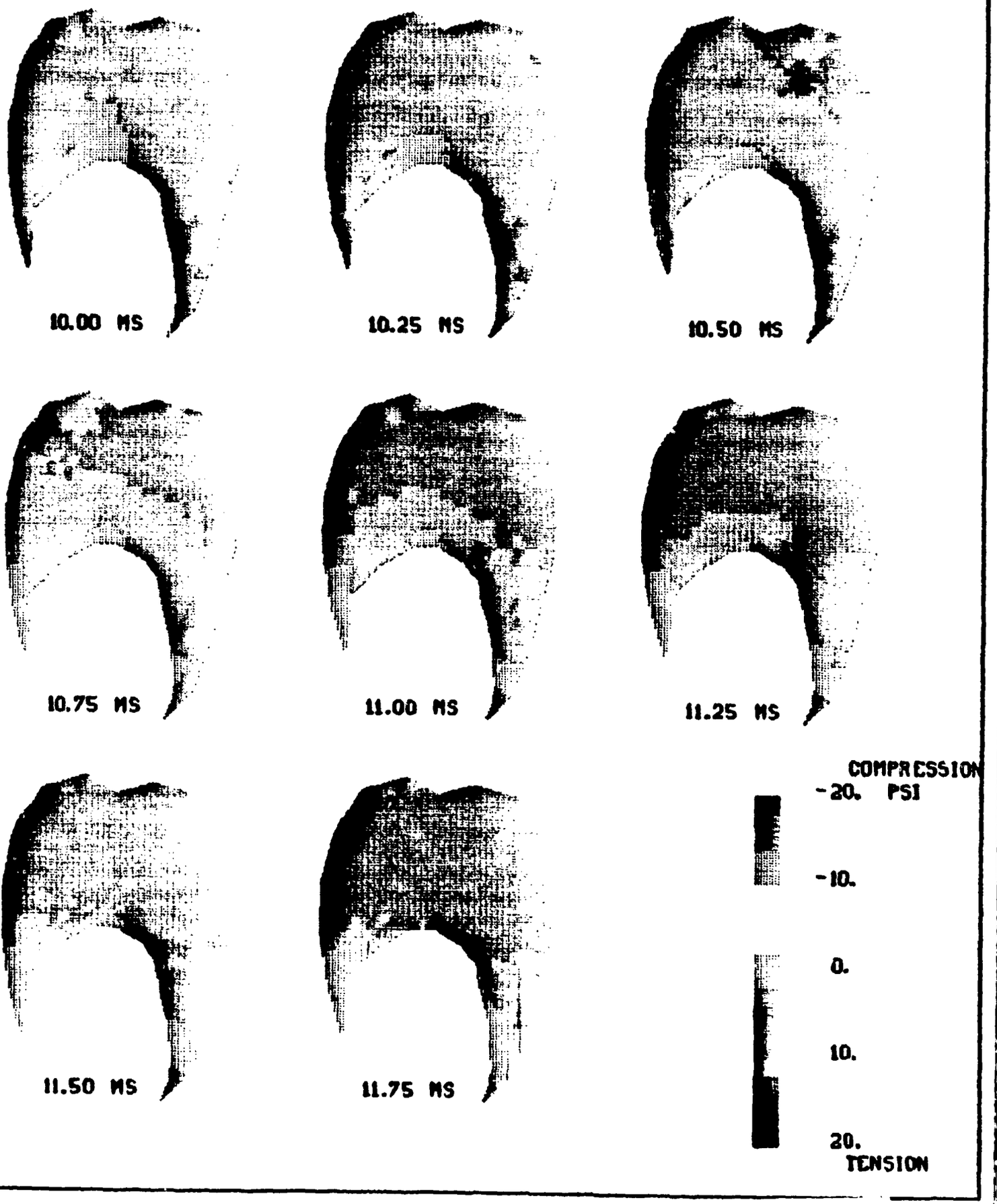

(f) Time 10.00-11.75 ms

Figure 3-2. (Cont'd)

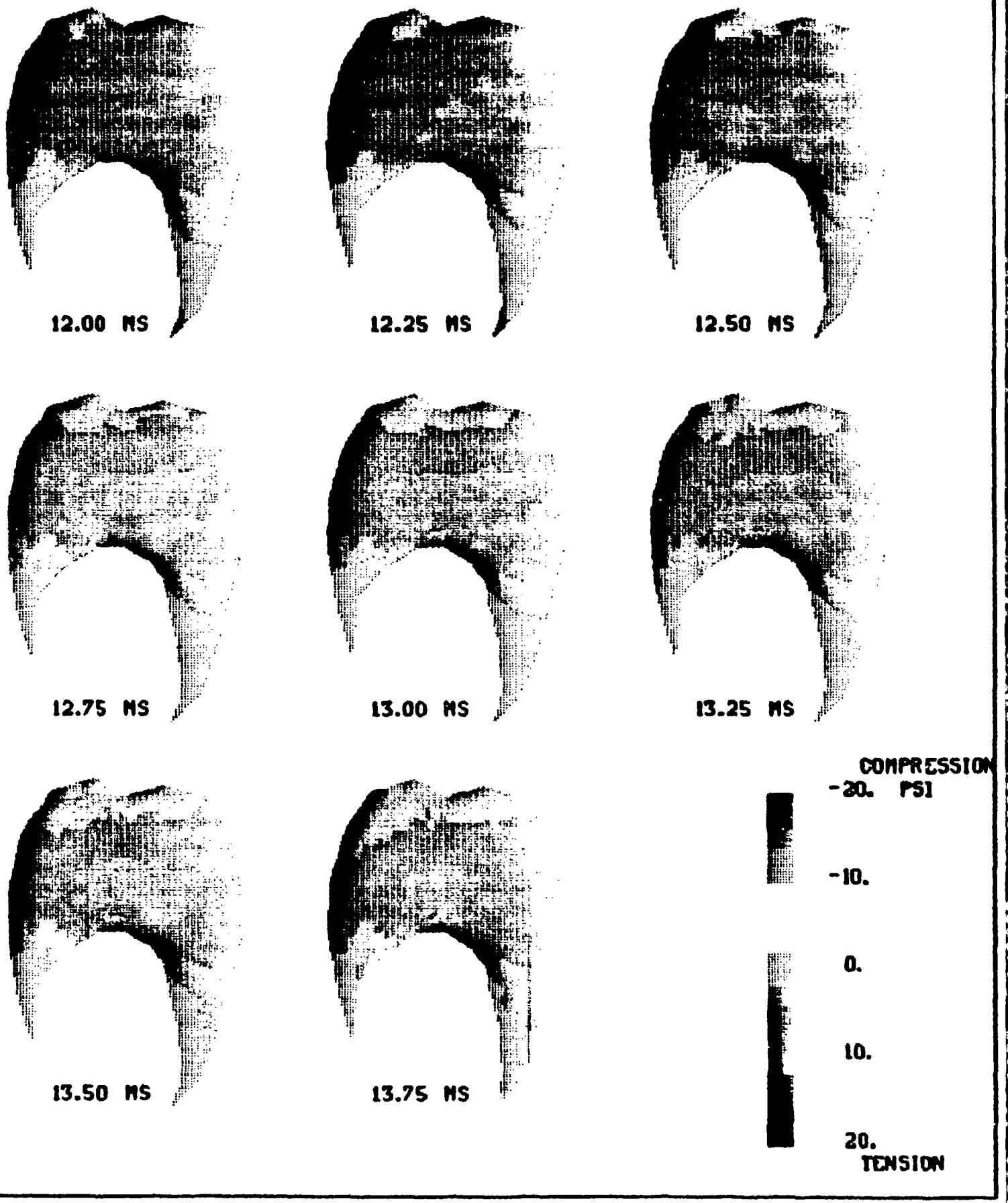

(g) Time 12.00-13.75 ms

Figure 3-2. (Cont'd)

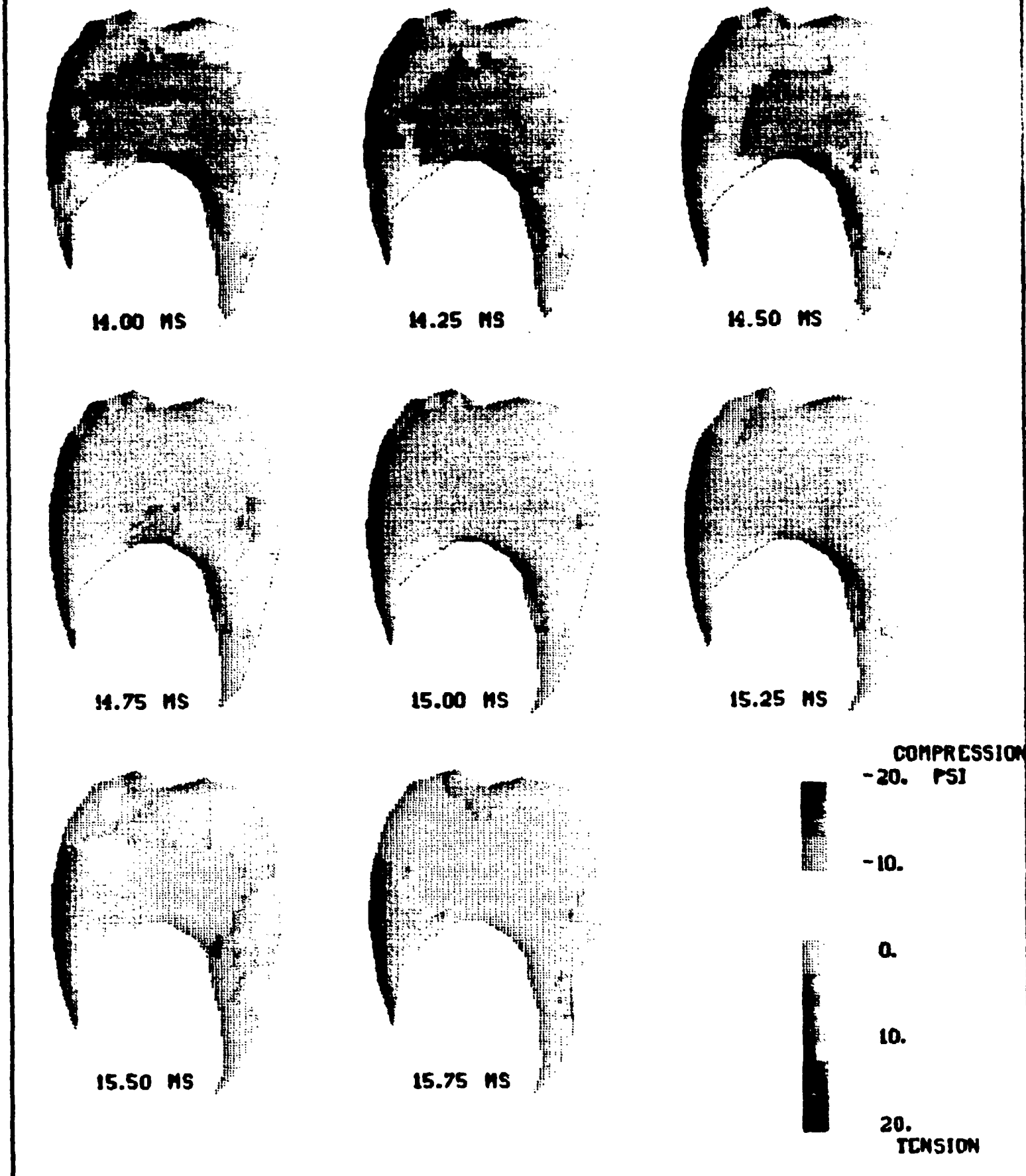

(h) Time 14.00-15.75 ms

Figure 3-2. (Cont'd)

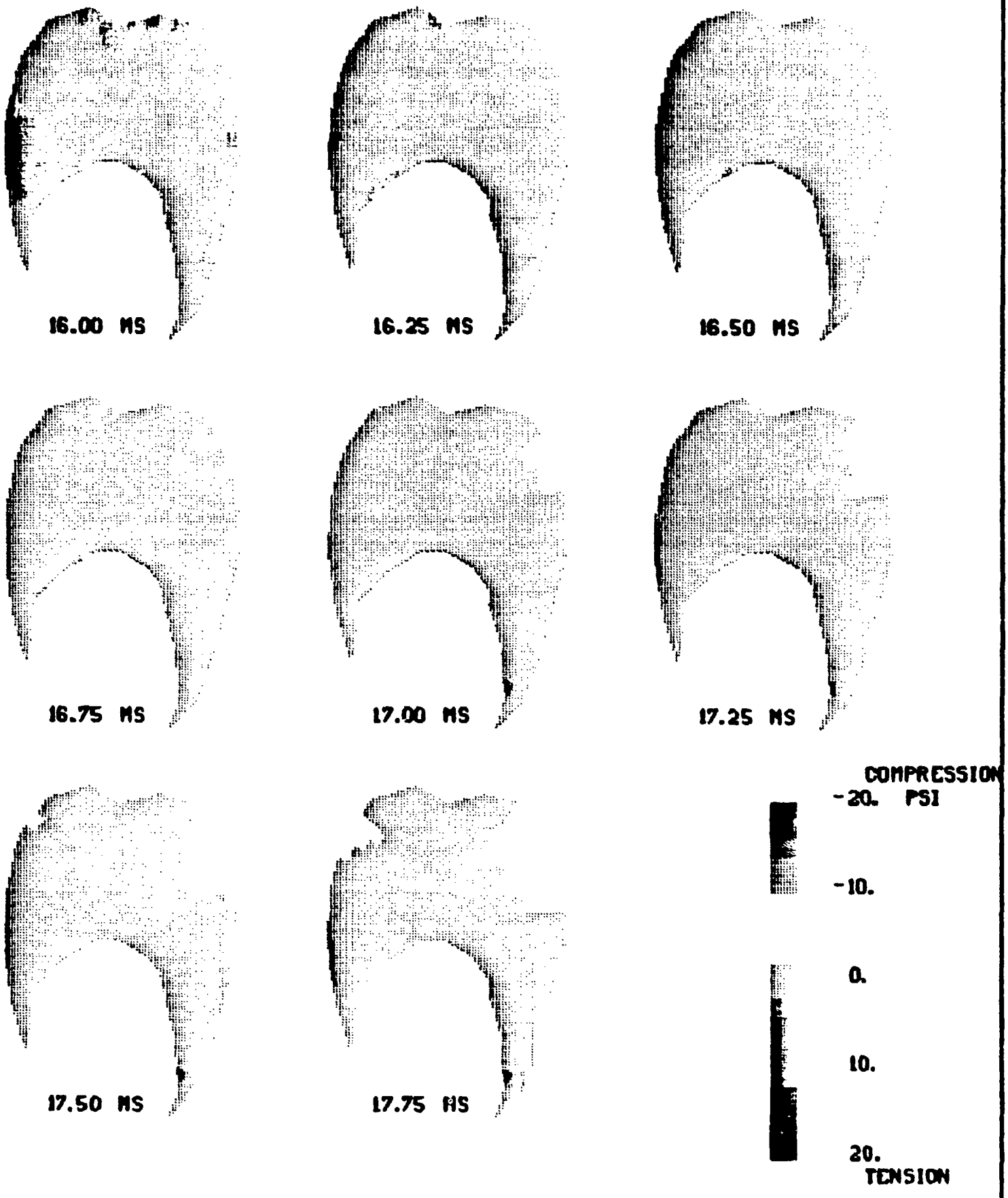

(i) Time 16.00-17.75 ms

Figure 3-2. (Cont'd)

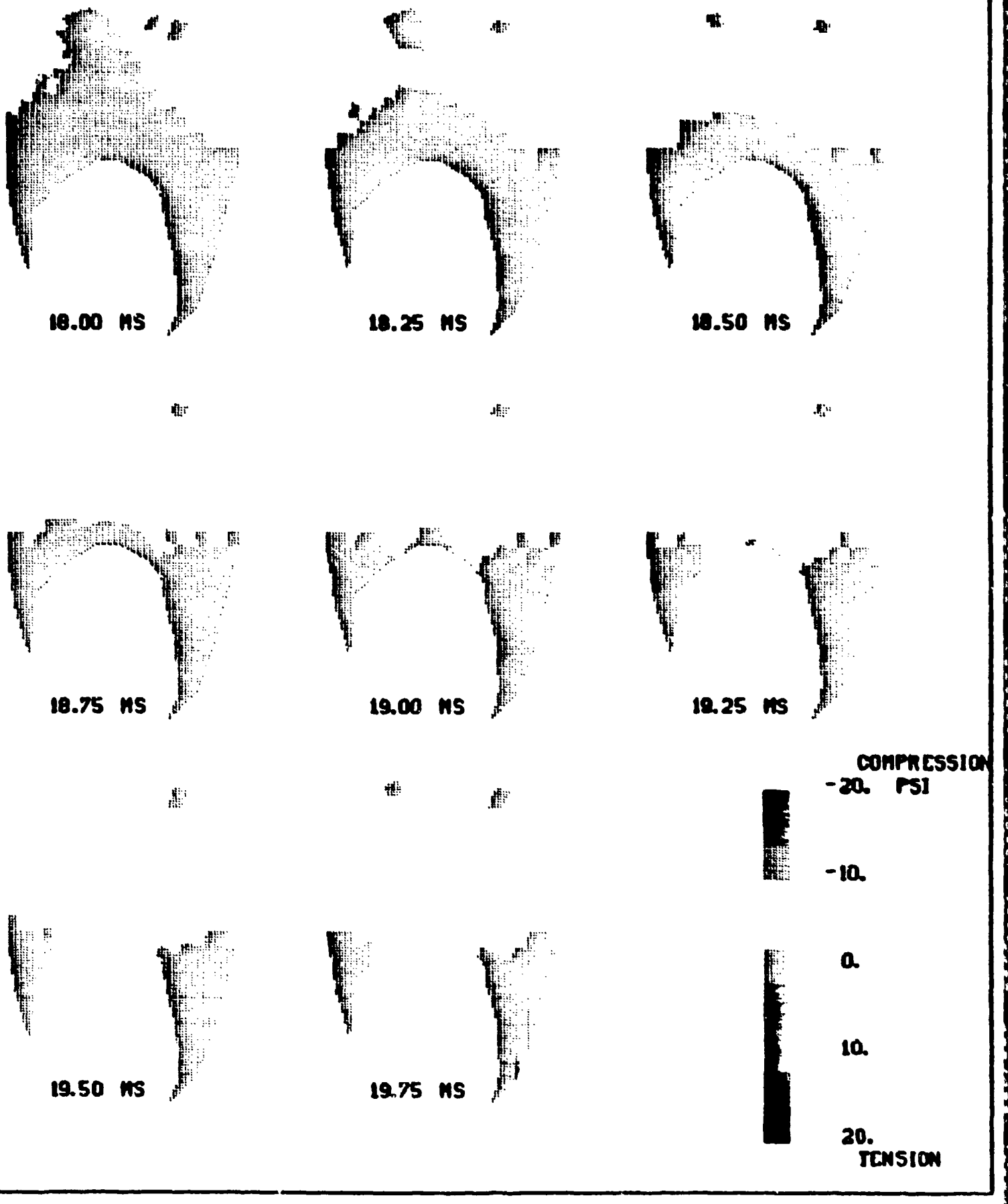

(j) Time 18.00-19.75 ms

Figure 3-2. (Cont'd)

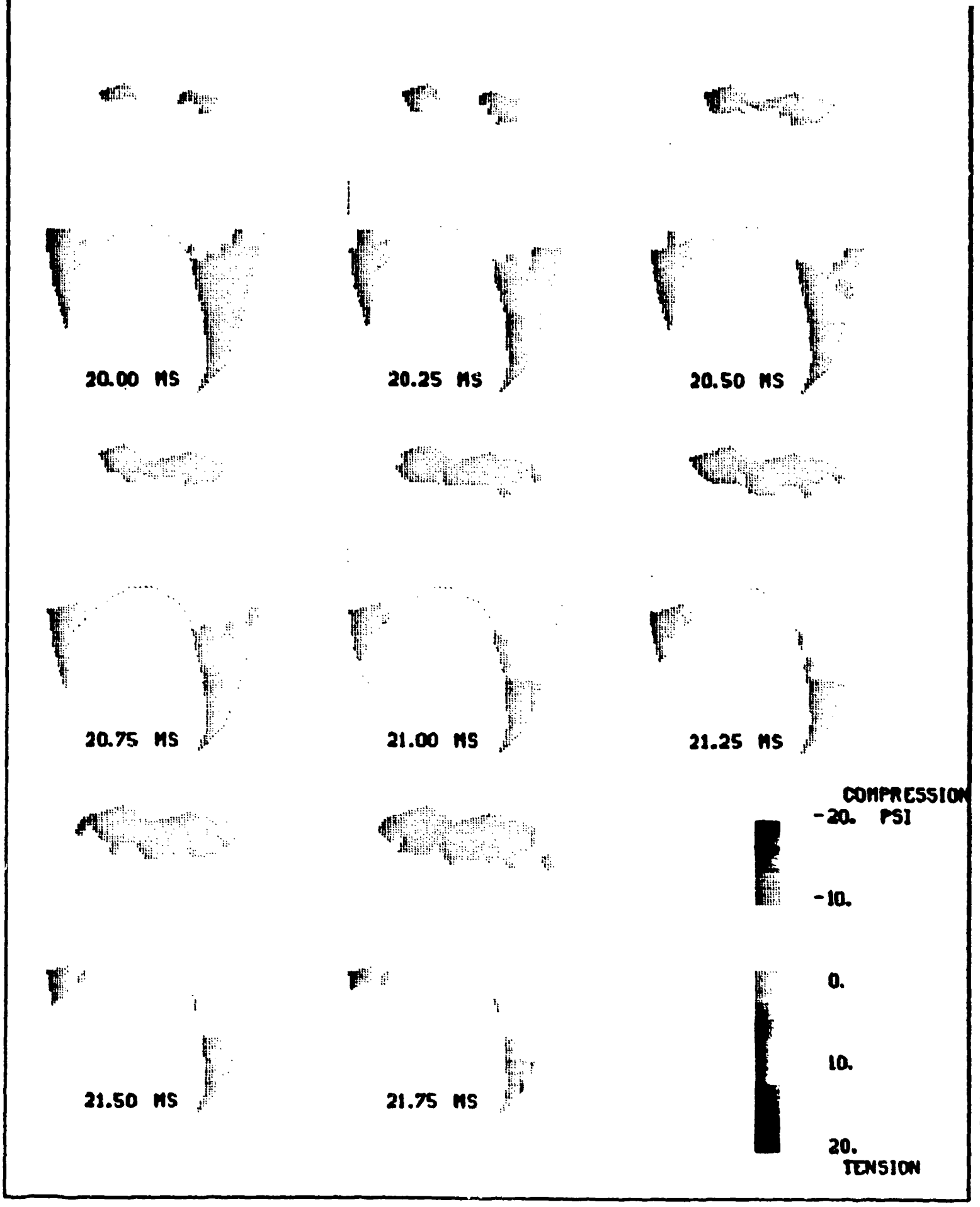

(k) Time 20.00-21.75 ms

Figure 3-2. (Cont'd)

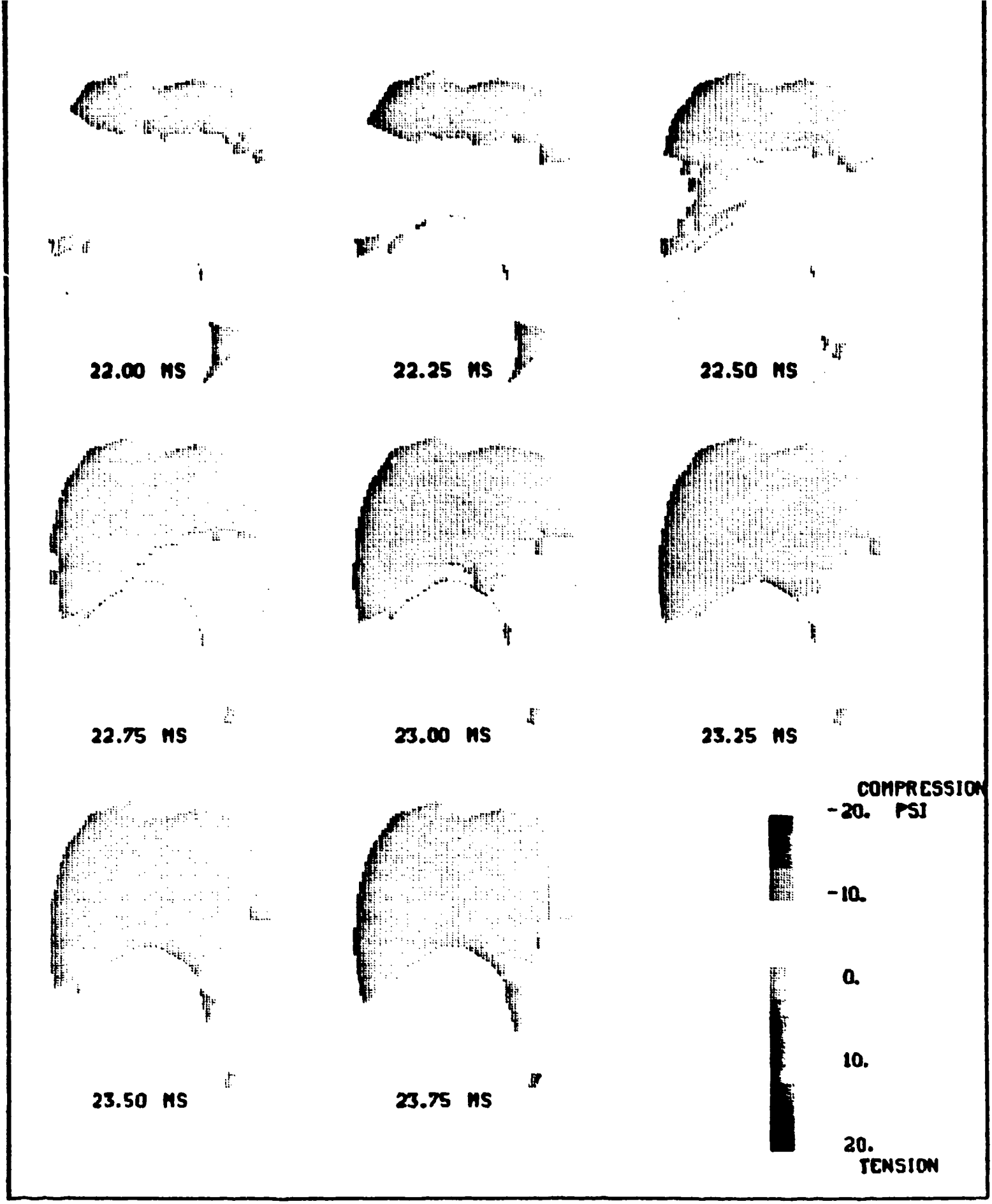

(1) Time 22.00-23.75 ms

Figure 3-2. (Cont'd)

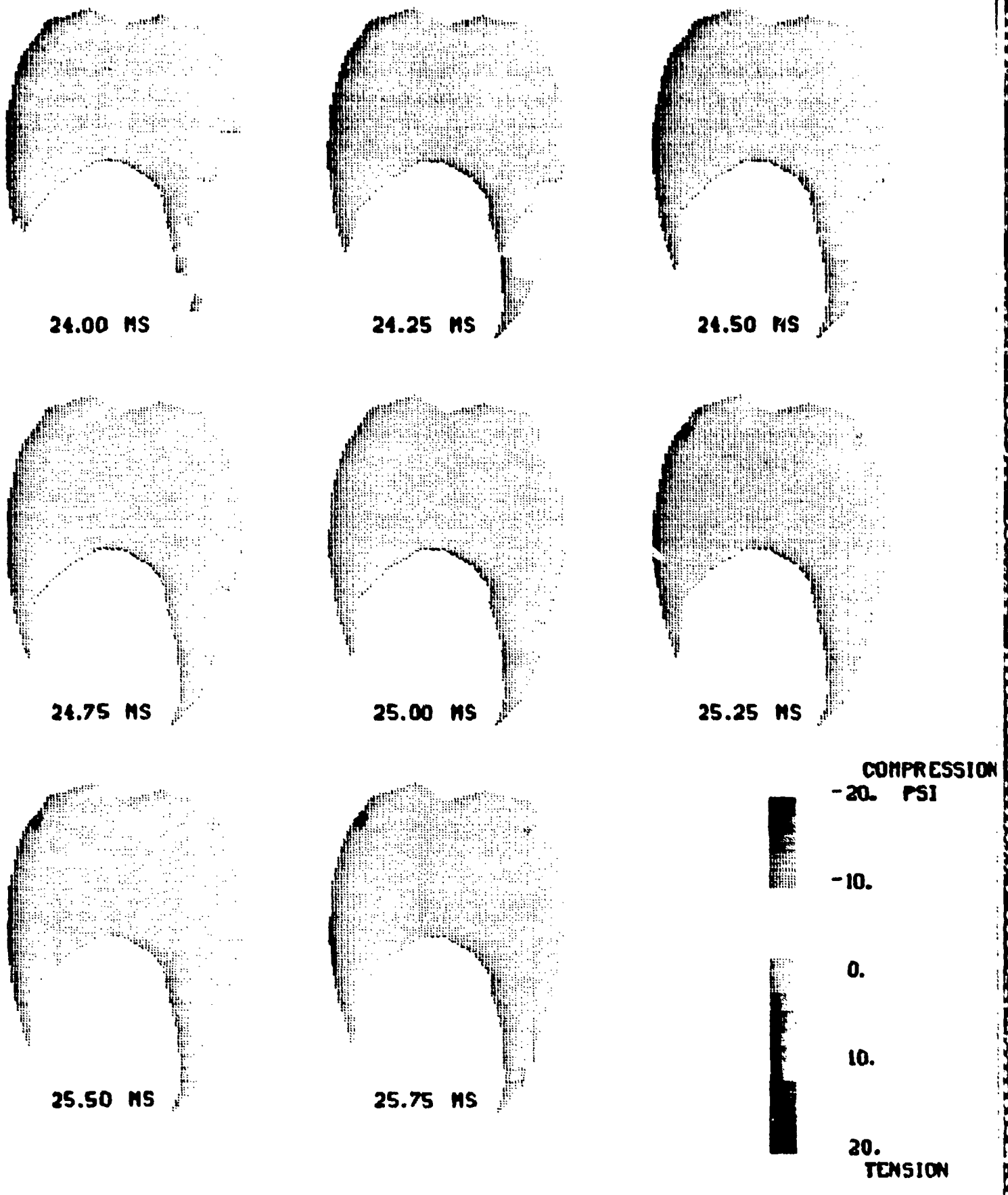

(m) Time 24.00-25.75 ms

Figure 3-2. (Cont'd)

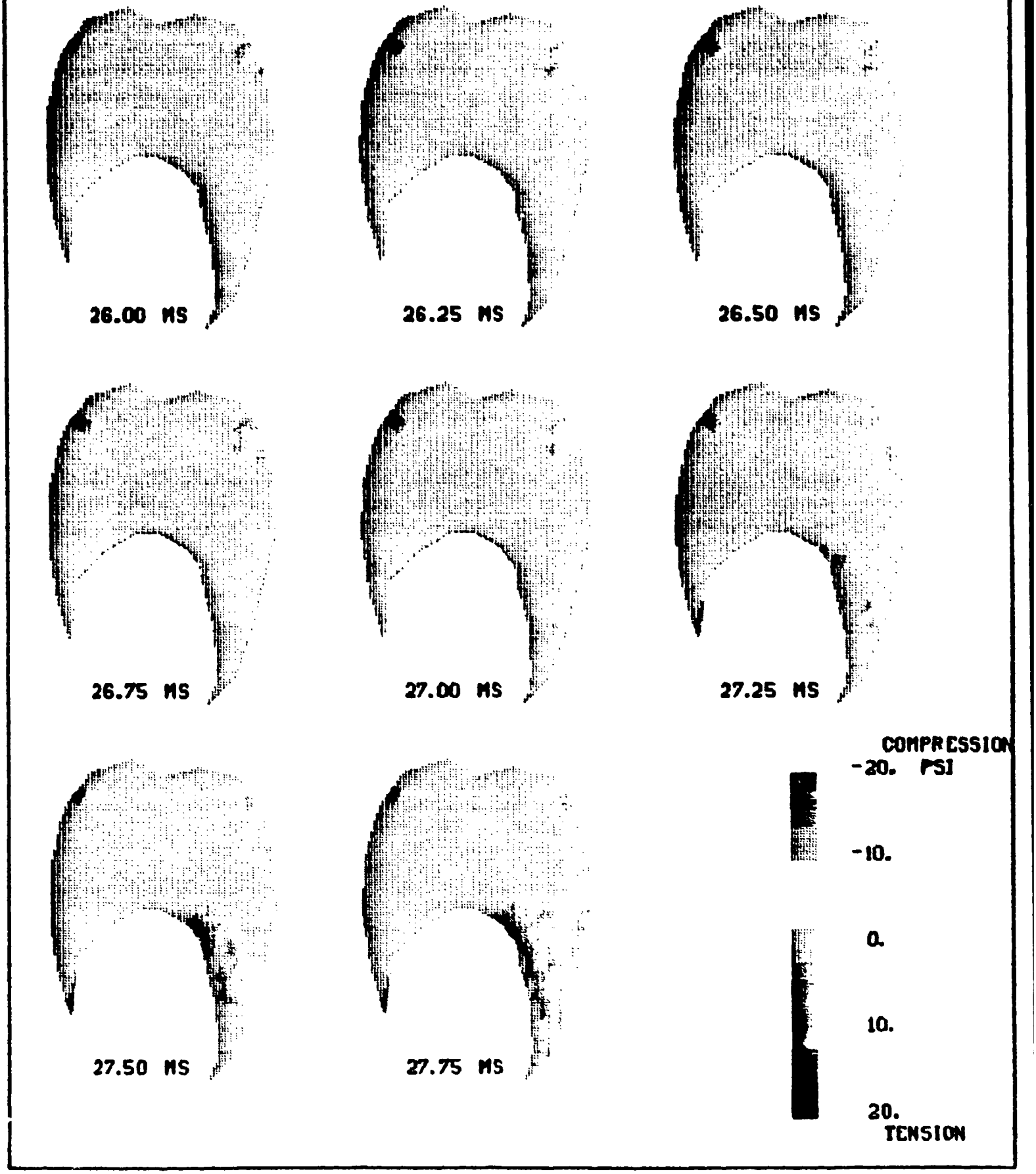

(n) Time 26.00-27.75 ms

Figure 3-2. (Cont'd)

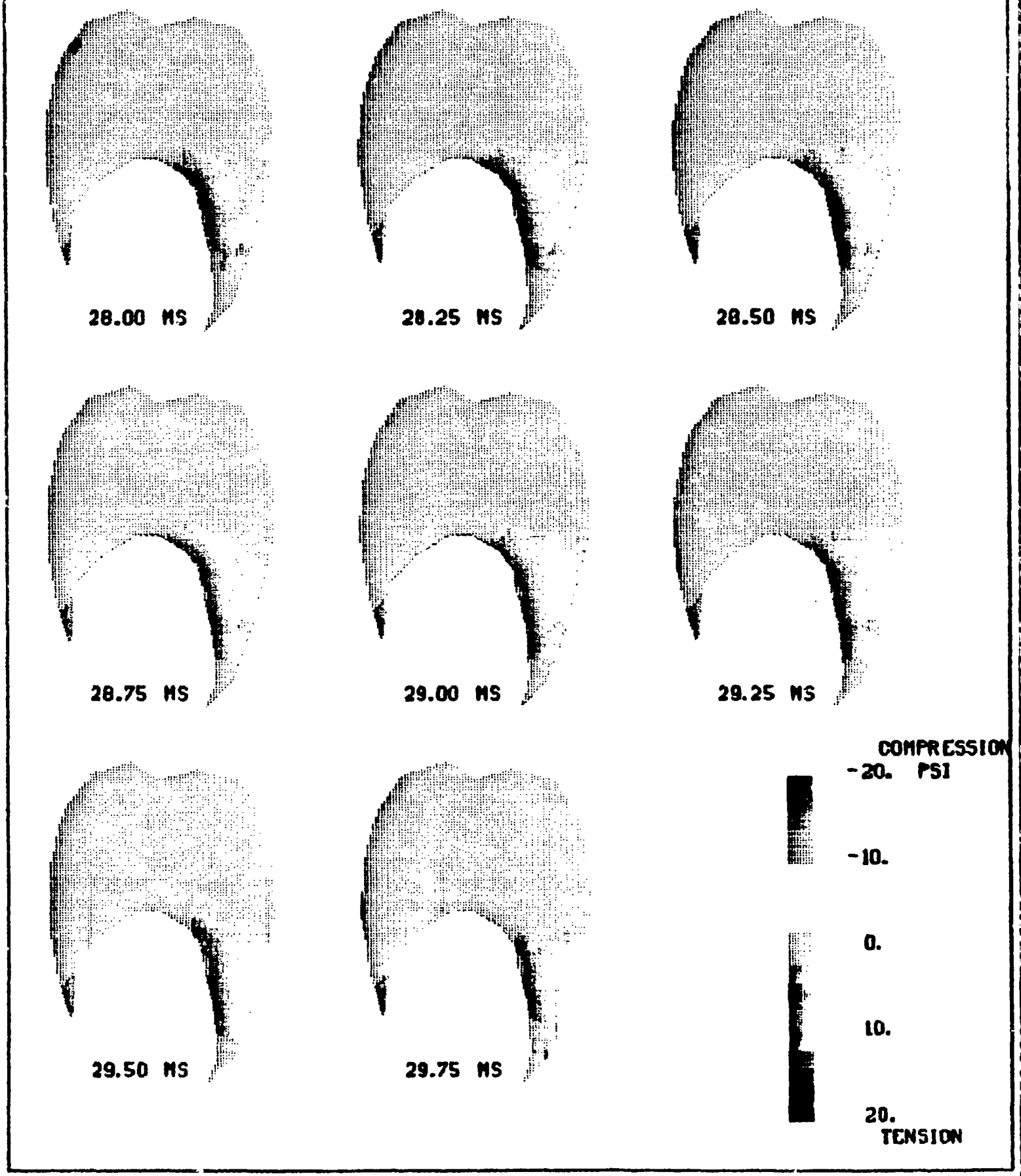

(o) Time 28.00-29.75 ms

Figure 3-2. (Cont'd)

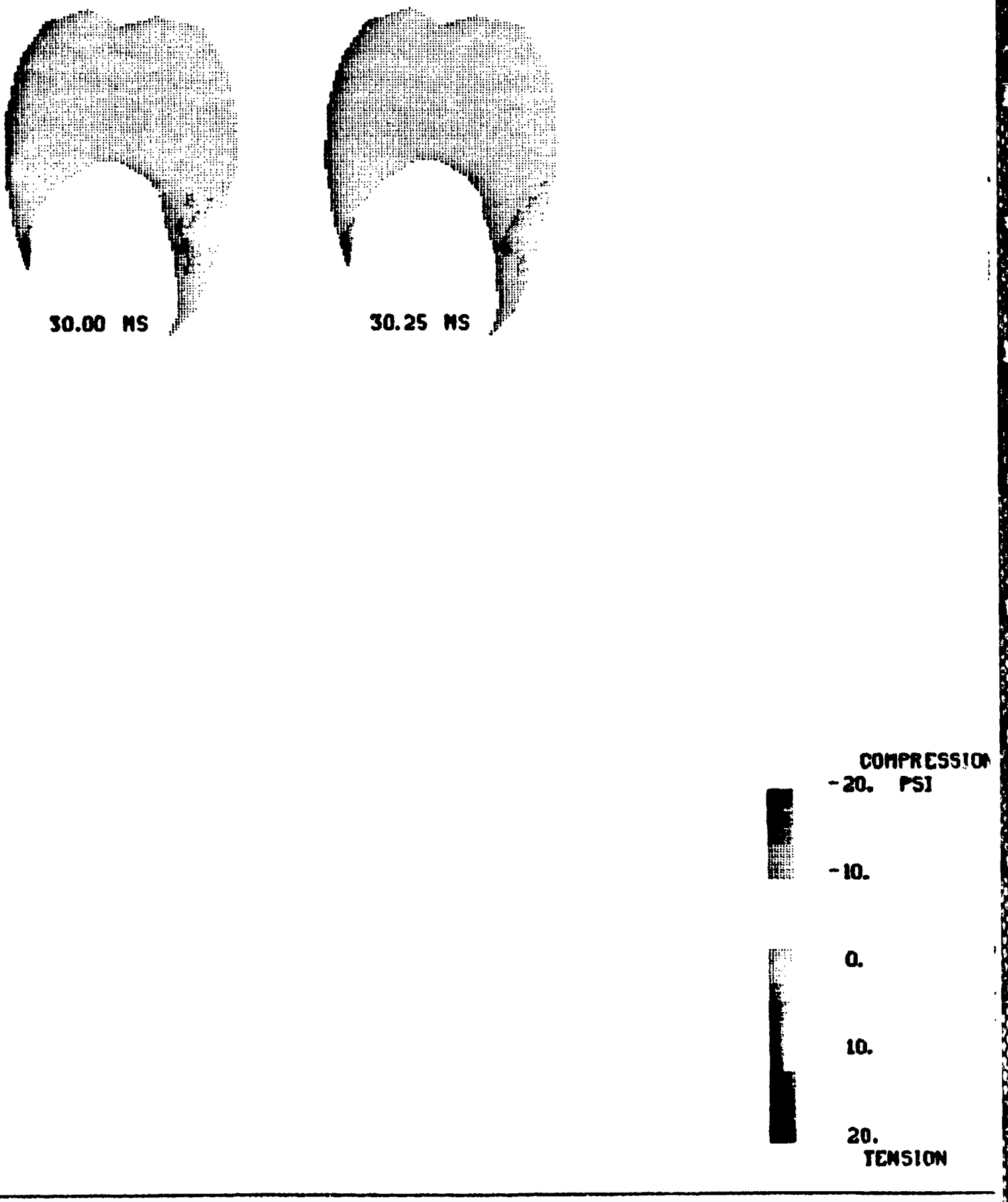

(p) Time 30.00-30.25 ms

Figure 3-2. (Cont'd)

pressure at the near myocardium wall. This local pressure increase is due to wave reflection.

5. As time goes by, compression waves entering from different parts of the body surface progress further to the center. At 3.75 through 4.0 ms they start merging at a region approximately the geometric center due to a focusing effect.

6. After passing each other, the wave fronts radiate away from the focal region. At time 5.25 through 5.5 ms, the stronger wave coming from the right side now reaches the left pleural surface. Reflection from the chest wall results in an overpressure increase at the left pleural surface. This does not occur at the other side, since waves coming from the left body surface are not as strong as those from the right, impact side.

7. Following this, the whole lung enters a tension phase. At 9.0 ms, we are able to see the gradual progression of the recoiled tension wave inside the lung. With the complicated geometry of the thoracic cavity, the wave motion in the lung becomes very complex.

8. At time 11.50-12.50 ms, the greatest magnitude of the tension wave occurs at the border near the pleural surface and the heart due to wave reflections from the "solid wall".

9. From 12.75-14.50 ms, the rebounded tension waves again merge at the region near the geometric focal point of the lung to result in a high tension. The relatively high tension at the border near the heart is probably due to the secondary reflection in addition to the component summed from the focusing effect.

10. Following 14.50 ms, the non-uniform oscillation of the waves continues with diminishing amplitudes. The analysis is extended up to 30.25 ms.

Wave speed in the lung has been measured to be in the range of 20-30 m/sec, which is much lower than the wave speeds in the skeletal muscle (1500 m/sec) and the bone (3000 m/sec) [3]. The low speed that waves travel in the lung lobes makes wave dynamics an important factor in causing damage. The complex environment of the thoracic cavity makes the wave motion inside the lung and its associated damage mechanisms complicated.

3.2 COMPARISON OF LUNG INJURY AND MODEL OVERPRESSURE PREDICTION

A comparison of FEM model ITP predictions, esophageal pressure measurements, and lung injury borderlines are shown on Figure 3-3(a) and (b). In terms of external peak blast overpressure, the maximum of model ITP

predictions are compared with experimental measured values [see Fig.3-3(a)]. The borderline for lung injury is identified as 17 psi. As the external peak blast is more than 41 psi, severe lung injury is reported [14]. Figure 3-3(b) shows similar comparison on the maximum of ITP increasing rate. These types of comparison provide us with first step correlation among external blast, animal response, and the resulting damage parameters.

With the finite element transient analysis we are able to capture the important wave features: focusing and reflection. It enables us to identify the occurrence of the high stress concentration in terms of timing and location. These regions are seen to correspond to, qualitatively, sites of observed lung hemorrhage following animal blast exposure.

Photographs (Fig. 3-4) taken from WRAIR sheep blast experiments were provided by Dr. Kenneth Dodd. Traumatized lungs were carefully removed from the animal after blast exposure for injury examination. These photographs show different degrees of lung injury due to blast wave exposure. On the top row, the animal was exposed to an airblast of 65 psi peak pressure. On the lower row, the sheep was exposed to an airblast of 50 psi peak pressure. Ventral and dorsal views are shown at the left and the right, respectively. Both cases show extensive areas of confluent hemorrhage on the intercostal surfaces. Some portions show the "rib marking" characterized by the dark red strips which extend deep into parenchyma from the surface. Serious hemorrhage is also seen at the lung pleuras bordering the heart. Ecchymotic spots are seen to scatter the rest of the lung surfaces.

Figure 3-5 shows maps of the maximal compression and tension any point in the lung experiences during the transient analysis. It appears that high compression occurs at the chest wave impact side. The narrow pleural region between the heart and the chest pleural surface also experiences very high compression. This is due to summation of the incident compression wave and the reflected component from the "firm organ" of heart. Similar high compression also occurs at the other side of the heart but not as seriously since the impact wave is not as strong as that at the right side. High compression at the geometric focal point is due to wave focusing effect. The high compression right above the heart can be due to the reflection and focusing effects. Distribution of maximum tension shows high tension occurs at the region near

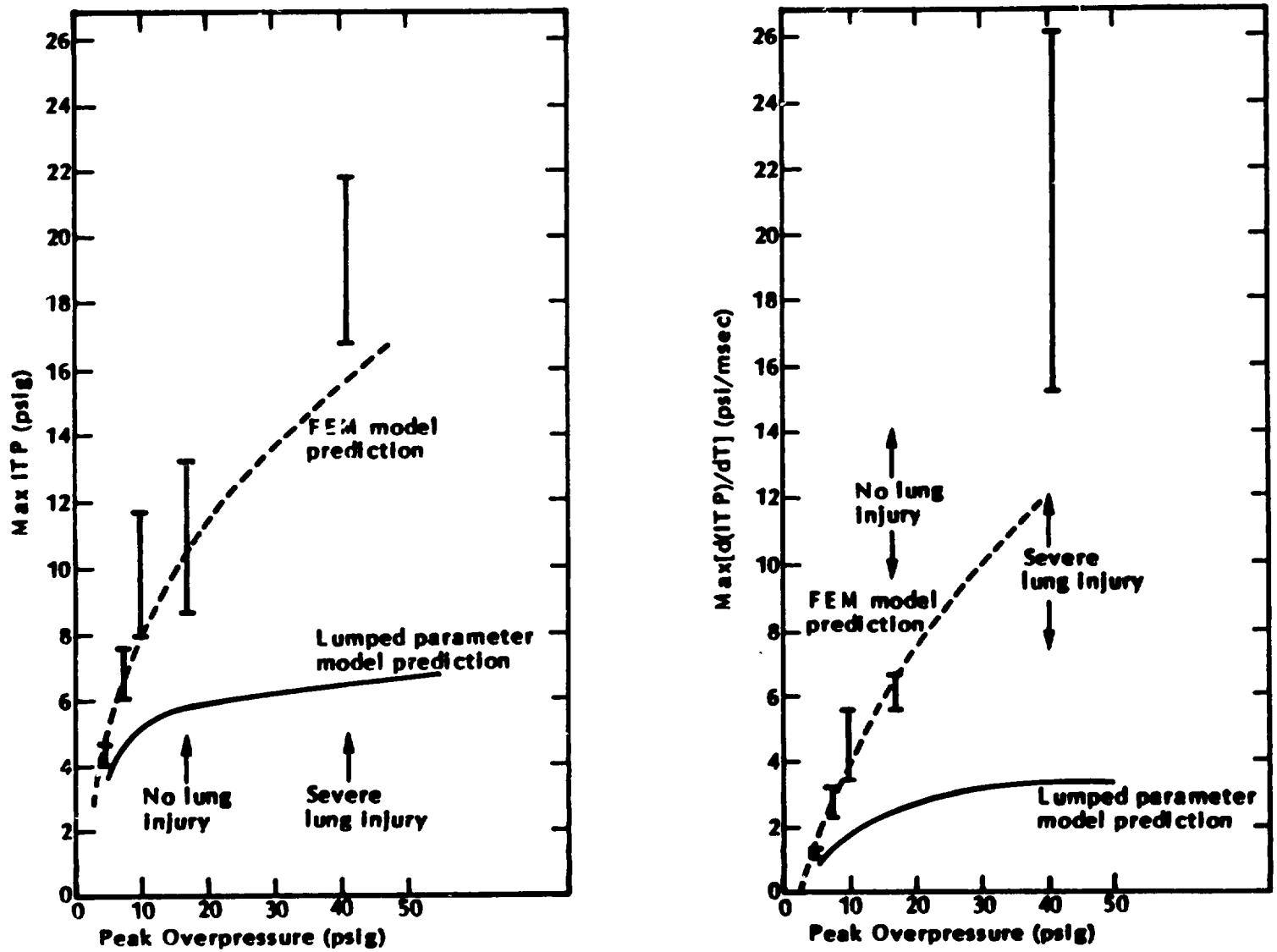

(a) Maximum ITP

(b) Rate of Maximum ITP Increase

Figure 3-3. Iso-impulse study comparison of the FEM model prediction with WRAIR experimental results.

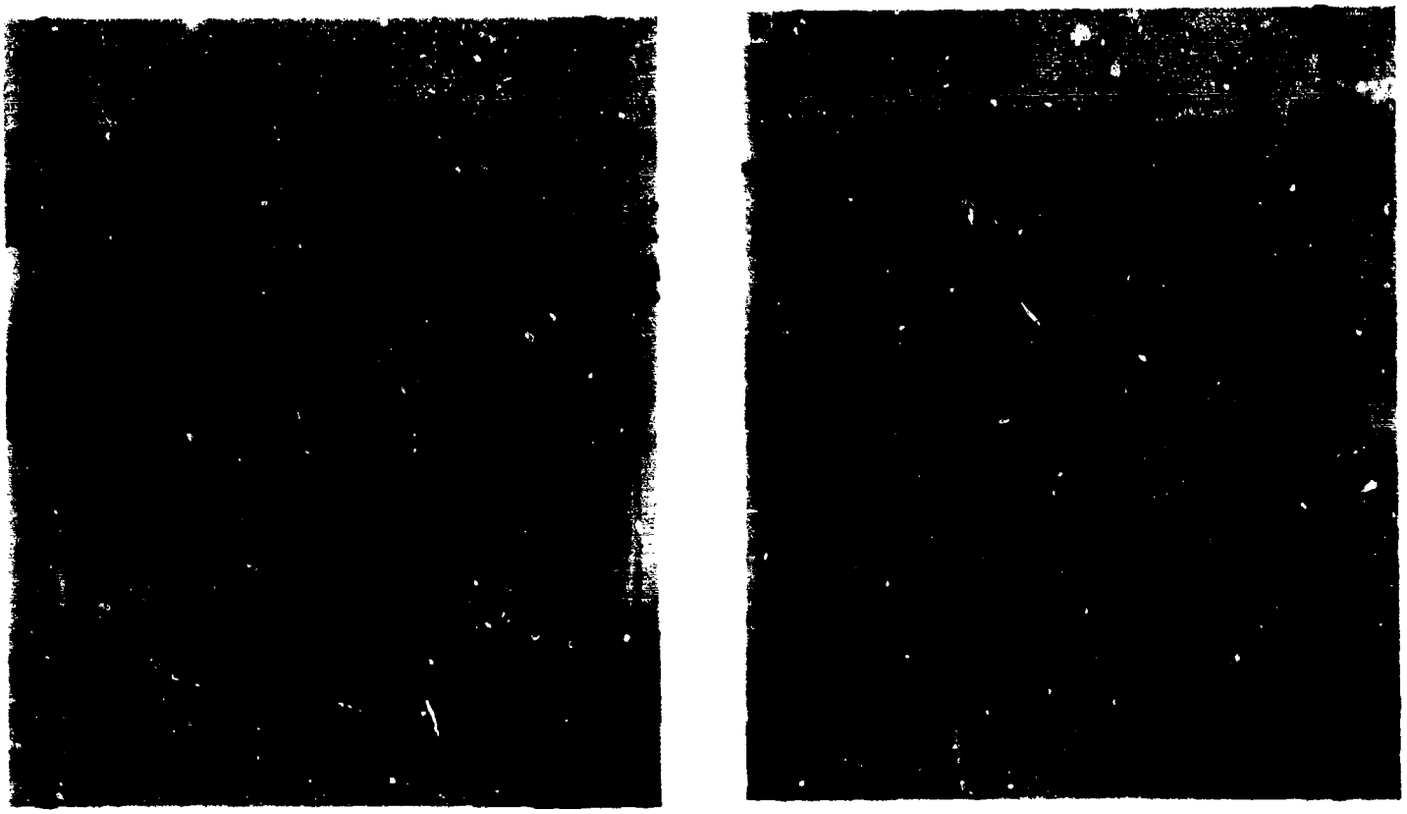

P_{peak} = 65 psi

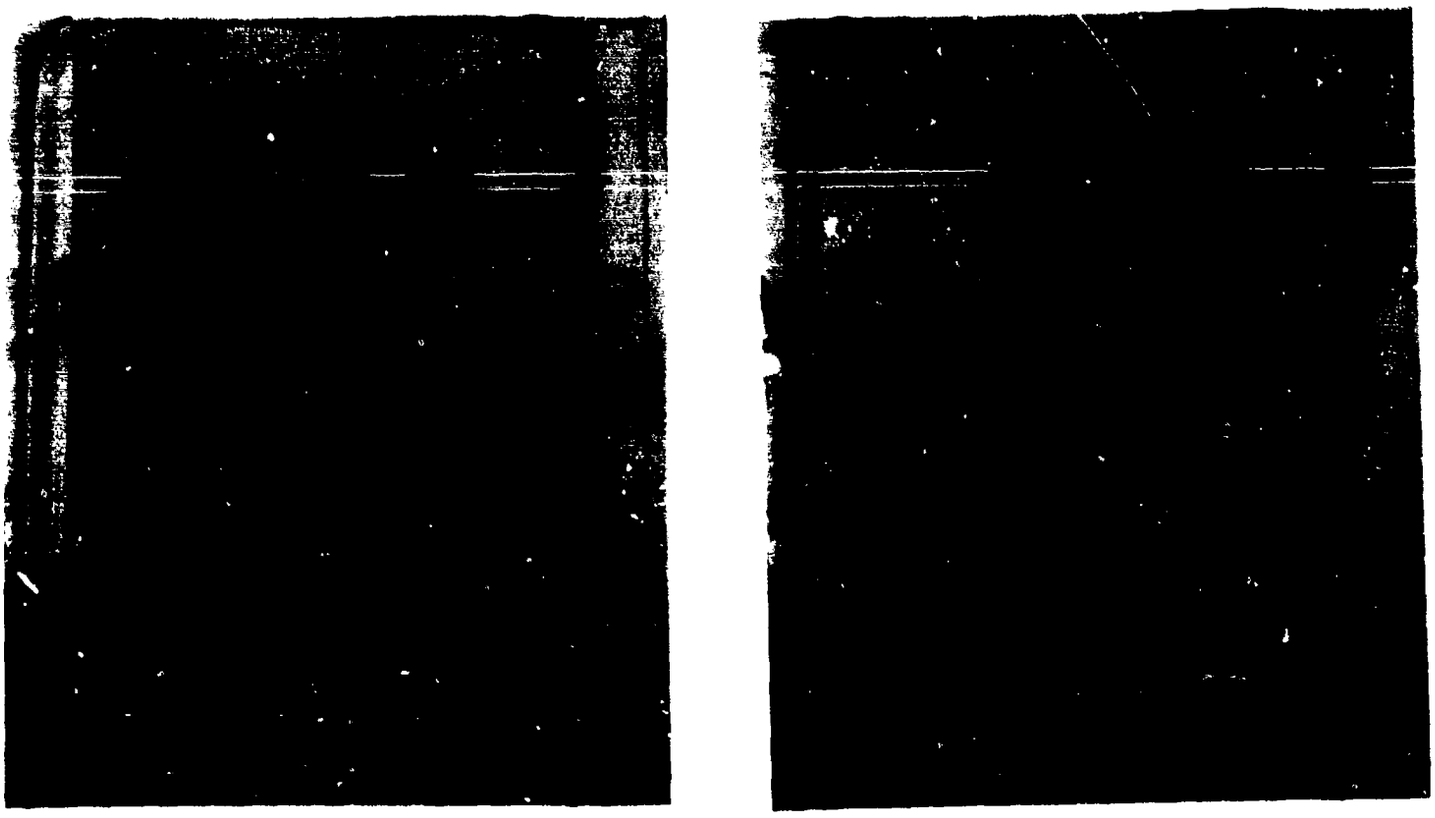

P_{peak} = 50 psi

Figure 3-4. Gross injuries on sheep lungs after blast wave exposures.

Figure 3-5. Maps of maximum compression and tension in the lung during the blast exposure of Figure 3-2.

the focal point, especially the part right above the heart. High tension is also predicted at the chest pleural surface of the wave impact side as well as the other side.

Comparison between traumatized lungs and model overpressure predictions shows that the chest pleural surface and the pleuras bordering the heart are the areas subject to most extensive hemorrhage and the highest overpressure loadings. The comparison is qualitative, yet it demonstrates the linkage between injury and local overpressure loadings.

Whether the lung damage of hemorrhage and edema, which mostly develop at a later time, are caused by the over-tension or overcompression is still a question needing more investigation. It can be achieved by spatial refinement of the model.

3.3 A LOCAL MODEL OF THE PLEURAL SURFACE WAVE DYNAMICS

Various experimental blast trauma studies indicate that hemorrhage usually starts at the superficial layer of the lung on the impact side. The term "rib marking" is commonly used to describe this type of hemorrhage. Zuckerman describes "spot of hemorrhage on lung surface, often following the lines of the ribs." For severe cases he describes, "rupture of visceral pleura, superficial lacer[illegible]ion along the lines of the ribs, occurrence of hemothorax and pneumothorax." The bony rib and intercostal muscle appear to provide different environments for the bordering lung tissue during blast. The lung tissue underneath the rib and the lung tissue underneath the intercostal muscle may experiences different pressures at wave reflection.

In order to better understand this fundamental phenomenon and its associated damage mechanism, an idealized local model of the pleural surface is used. The mo[illegible] con[illegible]s of a rib-muscle-lung structure.

The purpose of this model is to study the wave propagation characteristics at the chest pleural surface where materials of different mechanical impedance meet. As m[illegible]oned earlier, the low speed wave travels in the lung lobes compared to [illegible]e in muscle and bone, making wave transmission and reflection across the material interface an important factor in causing damage.

Two cases will be studied with this model. In the first case, the model is used to study the lung overpressure difference due to the presence of rib bone and intercostal muscle at the impact side. In the second case, the model is used to study the wave reflection characteristics from the pleural surface and its difference from the rib bone and intercostal muscle.

Case 1. The geometrical configuration of the model is shown at the center of Figure 3-6(a). Each of the small squares is a finite element in the model representation. The dimension of each element are one centimeter on a side. At the right end, the six black color elements represent the bony rib. The six elements right below the bone represent the intercostal muscle. At the far right, there is a layer of skeletal muscle. The rest of the elements with dot pattern represent the lung.

The wave loading is applied at the right end surface uniformly. The time variation of the pressure loading is shown in the subplot at the top of the center column. The loading has a peak pressure of 5 psi and a duration of 4.5 ms. Following the application of compression at the right end, the wave propagates toward the left. As indicated by arrows, each subplot depicts the pressure histories experienced by the local "lung tissue" (in the sense of a homogeneous continuum). At the right column of Figure 3-6(a) each of the subplots represents the overpressure responses at the pleural surface. It is seen that the lung parenchyma bordering the bone experiences higher overpressure response than that bordering the intercostal. For comparison these four curves are overlaid as shown in Figure 3-6(b). This type of response difference is not seen at interior points as shown on the four subplots at the left column of Figure 3-6(a). At the superficial layer the lung parenchyma bordering the bone is under more vigorous compression under wave incidence because of larger inertia of the bone. In response to blast waves, with the relatively high bulk moduli and incompressibility compared with the lung, the rib and muscle can be set into rigid body motion and move into the lung. The density of bone is reported to be from 2-2.9 gm/cm^3 [12], and the densities of muscle and lung parenchyma of large animals are approximately 1 and 0.2 gm/cm^3, respectively. Because of its greater inertia, the bone is harder to set into motion, but it will retain that motion and make a more effective indentation into the bordering lung parenchyma. This leads to a possible explanation of the rib markings observed by experimentalists and clinicians.

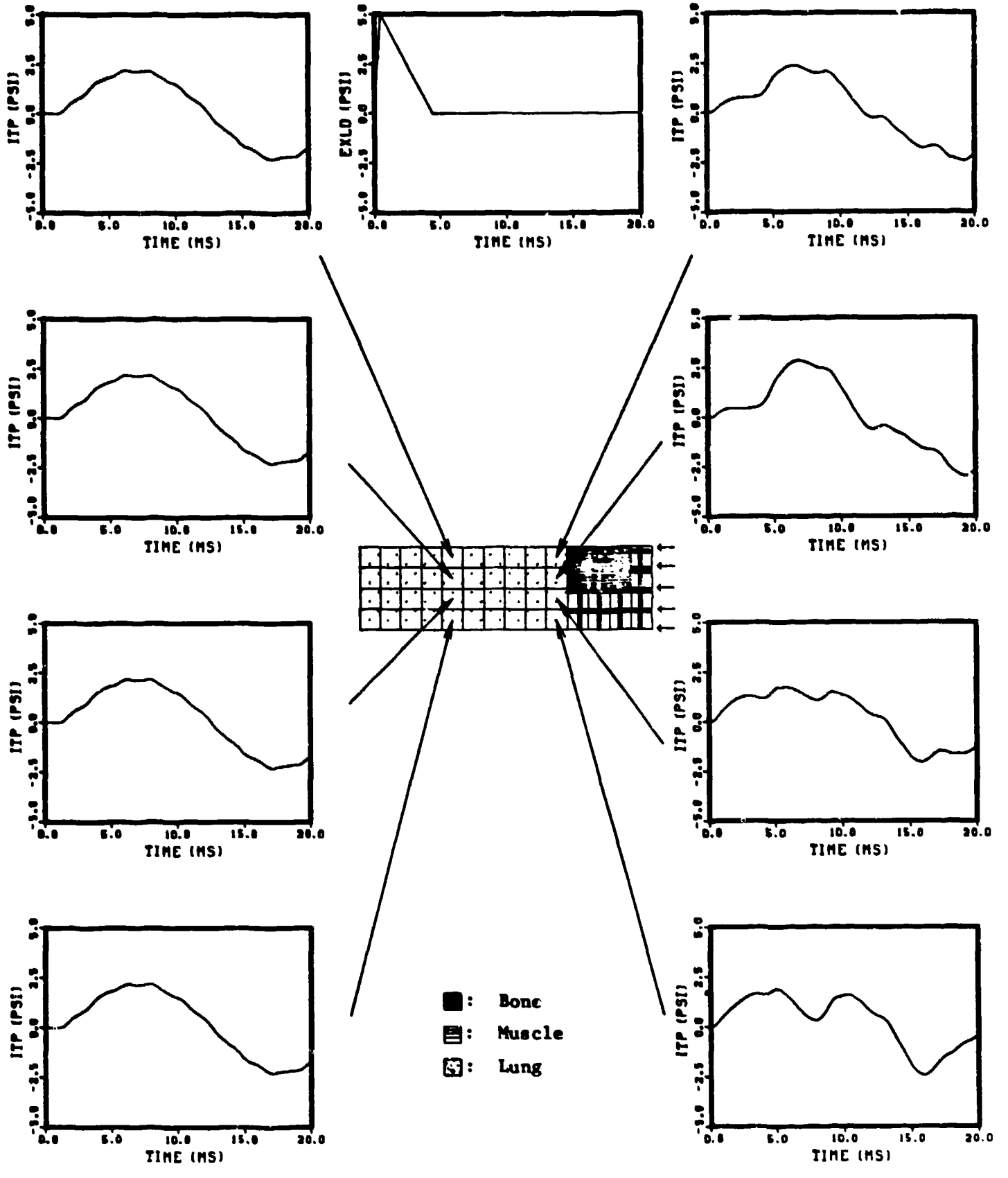

(a) Distribution of overpressure responses on an idealized bone-muscle-lung model

Figure 3-6. Overpressure responses.

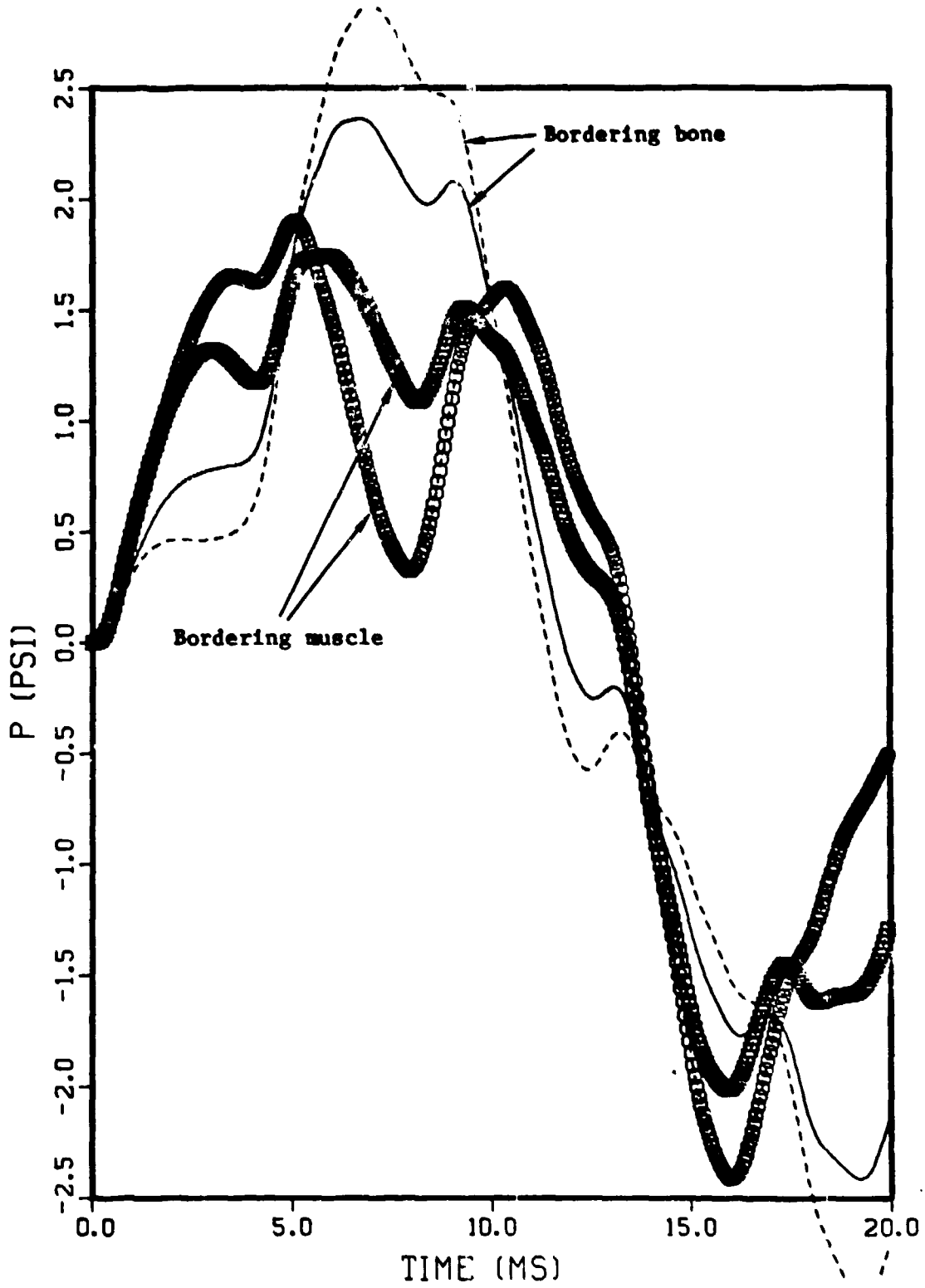

(b) Local overpressure differences at the region bordering the bone and the muscle

Figure 3-6. (Cont'd).

Case 2. The wave reflection characteristics from the chest pleural surface are studied. This analysis demonstrates the important wave reflection from a relatively solid wall and the non-uniform reflection from a rib bone and intercostal muscle. The model is shown at the center of Figure 3-7. The bone and the intercostal are each represented by two elements at the left end. The wave, which is already traveling in the lung region, approaches the pleural surface from the right. A Frelander type waveform is assumed (see the center top of Fig. 3-7).

Due to wave reflection from the relatively solid boundary, the lung tissue near the pleura is under increased stress magnitude. For a perfectly rigid boundary constraint, doubling effect should occur. The depth of the lung tissue layer under the increased stress magnitude depends on the frequency contents and the wave length of the incident wave. For a sharp-rising incident wave, a very acute stress increase could occur at the region close to the pleura. It is also noted that this local stress increase due to wave reflection occurs not only for the first incident compression wave, but also for the later rebounding waves.

For the given wave disturbance at the right end of the model, the overpressure responses at different points along the wave path are shown at subplots of Figure 3-7 as indicated. Different points along the wave path experience different overpressure histories. The closer to the firm wall the stronger the reflection occurs. Figure 3-8 shows the pressure differences at the pleural surface along the directions normal to the wave path. The four subplots at the left column show a pronounced stress increase at the layer immediately adjacent to the solid material. However, the lung tissue underneath the bone is predicted to experience a higher amplitude than that underneath the muscle. This is because the bone provides a more rigid constraint to the lung than the muscle does. Therefore, the stress increase due to the wave reflection is more effective at the lung right next to the bone. The more effective reflection at the lung adjacent to the bone occurs not only for the first incident wave but also for the rebounding waves arriving at a latter time. The stress increase due to wave reflection from a relatively rigid wall can further be enhanced for an inward-moving boundary wall.

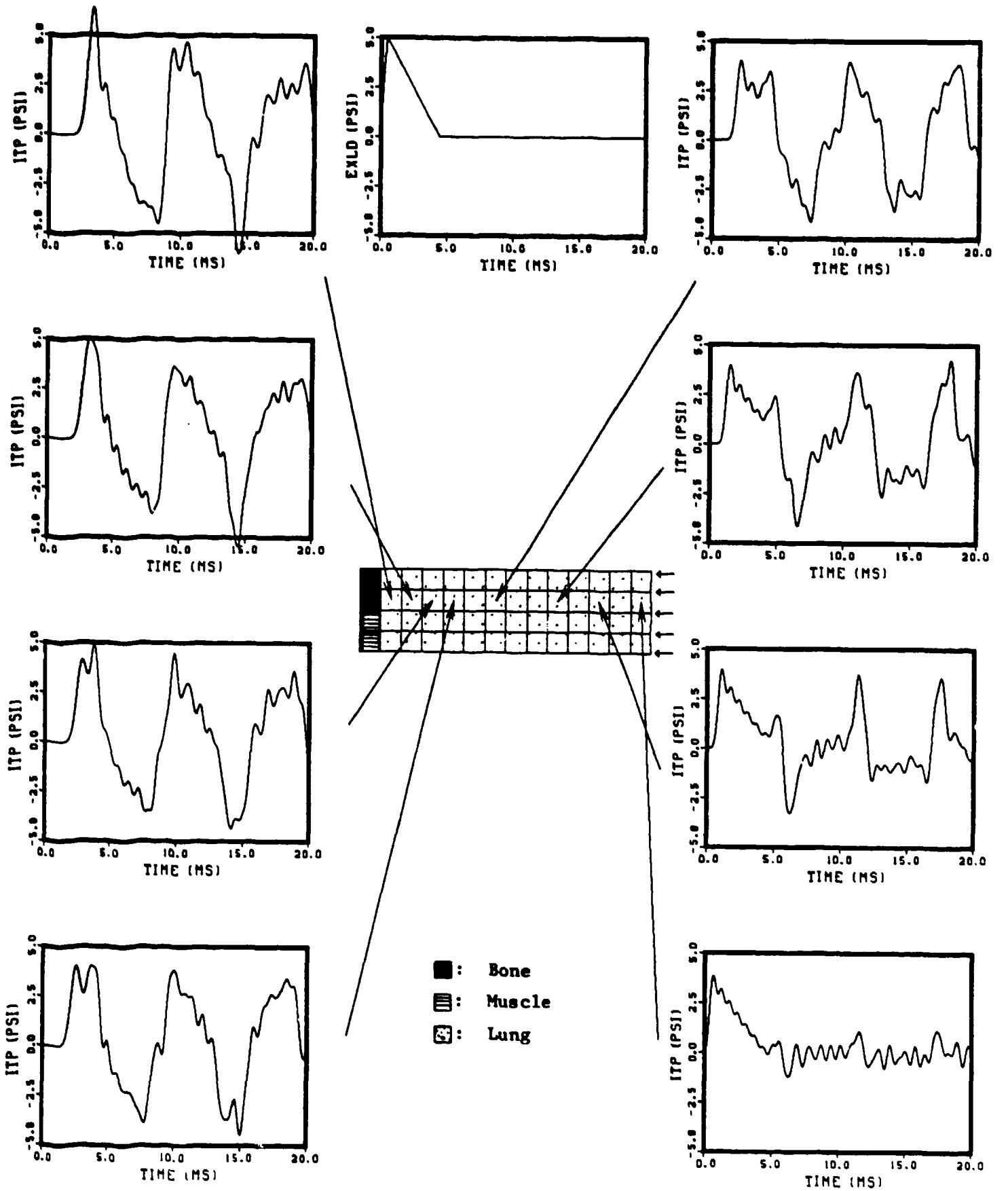

Figure 3-7. Different pressure responses along the wave path.

The four subplots at the right column of Figure 3-8, however, show similar pressure histories for the four elements far away from the pleura. This analysis demonstrates that the chest wall provides relatively solid wall to the lung in the thoracic cavity. Wave reflection from such a wall results in higher local stress at the superficial layer. At the border the bone provides a more effective solid wall than the muscle to result in a higher local overpressure. This also leads to a possible explanation of the origin of lung injury. It is consistent with the observation that (1) injury is always first seen from pleural surfaces, (2) the rib-marking type injury.

REFERENCES

1. Clemedson, C.-J., "Changes in Lung Elasticity in Air Blast Injury," Särtryck ur Försvarsmedicin 3, 100-106 (1967).

2. Desaga, H., "Blast Injuries," Chapter 14-D in German Aviation Medicine, World War II, 1274-1293, U. S. Government Printing Office, Washington, D.C. (1950).

3. Fung, Y. C. and M. R. Yen, "Lung Dynamics and Mechanical Properties Determination," a topical report to WRAIR under Contract No. DAMD-17-82-C-2062 (1983).

4. Jönsson, A., et al., "Dynamic factors influencing the production of lung injury in rabbits subjected to blunt chest wall impact," Aviat. Space Environm. Med. 50, 325-337 (1979).

5. Lau, V. K. and D. Viano, "Influence of Impact Velocity and Chest Compression on Experimental Pulmonary Injury Severity in Rabbits," J. Trauma, (21) 12: 1022-1028 (1981).

6. Lau, V. K., "Effect of Timing and Velocity of Impact on Ventricular Myocardial Rupture," J. Biomech. Engrg., (105): 1-5 (1983).

7. Life, J. S. and B. W. Pince, "Response of the Canine Heart to Thoracic Impact During Ventricular Diastole and Systole," J. Biomech., (1): 169-173 (1968)

8. Schardin, H., "The Physical Principles of the Effects of a Detonation," Chapter 14-A in German Aviation Medicine, World War II, 1207-1224, U. S. Government Printing Office, Washington, D. C. (1950).

9. Stein, P. D., et al., "Hepatic and Splenic Injury in Dogs Caused by Direct Impact to the Heart," J. Trauma, (23) 5: 395-404 (1983).

10. Webster, I. and L. J. Blum, "Traumatic Lung," Forensic Sci., (1): 167-178 (1972).

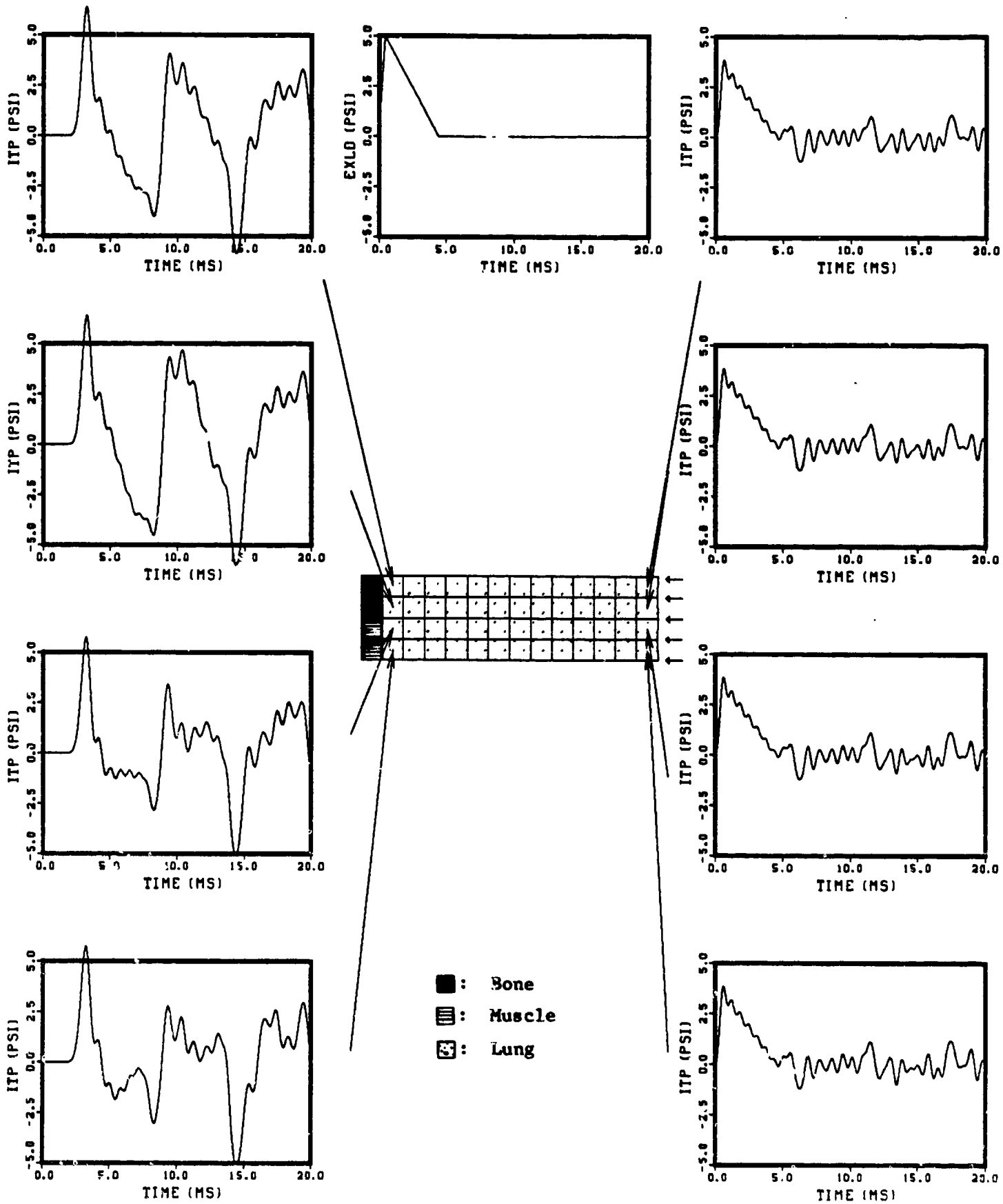

Figure 3-8. Pressure responses rear the pleural surface.

11. Zuckerman, S., "The Problem of Blast Injuries," Proc. Roy. Soc. Med. 34: 171-188 (1941).

12. Amtmann, E. and H. P. Schmitt, Z. Anat., 127: 25-41 (1968).

13. Chuong, C. J. and J. H. Stuhmiller, "Characterization and Modeling of Thoraco-Abdominal Response to Blast Waves, Volume 4: Biomechanical Model of Thorax Response to Blast Loading," Final Report to WRAIR under Contract No. DAMD17-82-C-2062 (1985).

14. Phillips, Y. Y., J. J. Jaeger, and A. J. Young, "Biophysics of Injury from Repeated Blast," Proceedings of Tripartite Technology Coordinating Program Panel W-2, Muzzle Blast Overpressure Workshop, May 1982.

DISTRIBUTION LIST

12 copies	Director Walter Reed Army Institute of Research Walter Reed Army Medical Center ATTN: SGRD-UWZ-C Washington, DC 20307-5100
1 copy	Commander US Army Medical Research and Development Command ATTN: SGRD-RMI-S Fort Detrick, Frederick, MD 21701-5012
12 copies	Defense Technical Information Center (DTIC) ATTN: DTIC-DDAC Cameron Station Alexandria, VA 22304-6145
1 copy	Dean School of Medicine Uniformed Services University of the Health Sciences 4301 Jones Bridge Road Bethesda, MD 20814-4799
1 copy	Commandant Academy of Health Sciences, US Army ATTN: AHS-CDM Fort Sam Houston, TX 78234-6100